# Graph-Based File Dispatching Protocol With D2D-Enhanced UAV-NOMA Communications in Large-Scale Networks

Baoji Wang<sup>®</sup>, Rongqing Zhang<sup>®</sup>, *Member, IEEE*, Chen Chen, *Senior Member, IEEE*, Xiang Cheng<sup>®</sup>, *Senior Member, IEEE*, Liuqing Yang<sup>®</sup>, *Fellow, IEEE*, Hang Li<sup>®</sup>, and Ye Jin

Abstract—As a newly emerging communication assistant equipment, unmanned aerial vehicles (UAVs) can be exploited to dispatch data files quickly to specific areas and support rapid deployment of communication links in complex terrain, which is of great significance for specific communication demands in disaster and remote areas. Nonorthogonal multiple access (NOMA), as a rosy technology in the fifth generation (5G) and future mobile communication systems, has been widely studied because of its ability in improving spectral efficiency and reducing transmission latency to enhance the overall Quality of Service (QoS) and meet the strict communication requirements. Based on these, in this article, we propose a device-to-device (D2D)-enhanced UAV-NOMA network architecture, in which D2D is introduced to increase the file dispatching efficiency. In our proposed D2Denhanced UAV-NOMA network, the ground users (GUEs) that have already received file blocks (FBs) are allowed to reuse the time-frequency resources assigned to NOMA links to share their FBs with other GUEs, which significantly improves the efficiency of file dispatching. But this also leads to a complicated interference environment. In order to effectively manage the interference and minimize the UAV-assisted file dispatching mission time, we propose a graph-based file dispatching (GFD)

Manuscript received October 30, 2019; revised February 27, 2020, April 6, 2020, and April 20, 2020; accepted April 30, 2020. Date of publication May 15, 2020; date of current version September 15, 2020. This work was supported in part by the Ministry National Key Research and Development Project under Grant 2017YFE0121400, in part by the National Science Foundation under Grant CNS-1932413 and Grant ECCS-1935915, in part by the National Natural Science Foundation of China under Grant 61901302, in part by the Open Research Fund of National Mobile Communications Research Laboratory, Southeast University under Grant 2020D01, and in part by the Open Research Fund from Shenzhen Research Institute of Big Data under Grant 2019ORF01006. (Corresponding author: Rongging Zhang.)

Baoji Wang is with the State Key Laboratory of Advanced Optical Communication Systems and Networks, Department of Electronics, School of Electronics Engineering and Computer Science, Peking University, Beijing 100871, China, and also with the National Mobile Communications Research Laboratory, Southeast University, Nanjing 211189, China (e-mail: bjwang@pku.edu.cn).

Rongqing Zhang is with the School of Software Engineering, Tongji University, Shanghai 201804, China, and also with the National Mobile Communications Research Laboratory, Southeast University, Nanjing 211189, China (e-mail: rongqingz@tongji.edu.cn).

Chen Chen, Xiang Cheng, and Ye Jin are with the State Key Laboratory of Advanced Optical Communication Systems and Networks, Department of Electronics, School of Electronics Engineering and Computer Science, Peking University, Beijing 100871, China (e-mail: c.chen@pku.edu.cn; xiangcheng@pku.edu.cn; jinye@pku.edu.cn).

Liuqing Yang is with the Department of Electrical and Computer Engineering, Colorado State University, Fort Collins, CO 80523 USA (e-mail: lqyang@engr.colostate.edu).

Hang Li is with the Data-Driven Information System Laboratory, Shenzhen Research Institute of Bid Data, Shenzhen 518172, China (e-mail: hangdavidli@163.com).

Digital Object Identifier 10.1109/JIOT.2020.2994549

protocol, in which the complicated joint optimization problem is decomposed to be solved efficiently and graph theory-based algorithms are proposed for resource allocation. The simulation results verify the advantages of our proposed D2D-enhanced UAV-NOMA network architecture and the efficiency of our designed GFD protocol in minimizing the total UAV-assisted file dispatching mission time.

Index Terms—Device to device (D2D), file dispatching, nonorthogonal multiple access (NOMA), unmanned-aerial-vehicle (UAV) communications.

#### I. Introduction

N RECENT years, the application of unmanned aerial vehicles (UAVs) has explosive growth, especially in the military and commercial fields. Various implementations of UAVs have gradually emerged in the civil field as well. In some places, where traditional terrestrial transportation is inconvenient or where natural disasters occur, UAVs can be deployed rapidly and complete various missions, such as reconnaissance, surveillance, mapping, and disaster rescue [1].

In addition to these applications, UAV-assisted communications have been of particular interest owing to its significant advantages. Compared with the terrestrial communication systems, the deployment of UAVs is more convenient and flexible. Communication links can be quickly established by the UAVs, which eliminates the wiring link on the ground [2], [3]. The UAVs can be flexibly deployed or recycled when working as mobile base stations (MBSs) for file dispatching to solve the tide effect of business demand and reduce network costs. Meanwhile, UAV-assisted communication systems may have wider coverage and better channel conditions because the UAVs are more likely to have line-of-sight (LOS) links when flying above the ground users (GUEs) as an MBS [4], [5]. The 3rd Generation Partnership Project (3GPP) has already proposed various possibilities of the UAV-assisted communications and carried out a series of relevant researches, since 2017 in the release R15 [6], [7]. For many of the applications in the Internet of Things (IoT) such as information broadcasting/multicasting, where the target users/nodes are quasistationary, UAV-aided communications can really improve the flexibility and efficiency of completing the mission [8]. An example is a scenario that the vehicles in large parking lots have the request for preloading data files, which can be maps

2327-4662 © 2020 IEEE. Personal use is permitted, but republication/redistribution requires IEEE permission. See https://www.ieee.org/publications/rights/index.html for more information.

or media data, or the scenario that edge computing is applied to fully utilize the computational resources of the vehicles in parking lots [9]–[11]. UAV-aided communications can be used as the supplement or offloading of traditional communication networks [12], [13].

Power-domain nonorthogonal multiple access (NOMA) is a promising key multiple access technology in the fifth-generation (5G) communication systems [14], [15]. The main idea of NOMA is to realize multiple access through different power levels via the same time–frequency resource block (RB), which can improve the spectral efficiency and access quantity. Thus, NOMA meets the explosive data growth and access demand of 5G systems [16], [17]. Since NOMA is suitable for the future system deployment [18], [19], it becomes fashionable to adopt NOMA in UAV-assisted communication networks for file dispatching.

Considering the advantages of NOMA, we apply NOMA in the UAV-assisted communication systems to support multicast services. The requested data files can be dispatched with the help of NOMA, which can improve the transmission efficiency, save the UAV's energy, and reduce the mission latency. In order to utilize the UAV's flying time effectively and further improve the system performance, the device-to-device (D2D) communication technique is adopted among the GUEs to share the received data files. D2D communications have been considered to be an effective way of cellular data offloading [20], [21]. With appropriate resource management and power control, the D2D links can reuse the same resources with the NOMA links based on spatial reuse to reduce the transmission load of the NOMA-based file downloading and further reduce the mission latency [22], [23].

In this article, we investigate the mission latency minimization problem of UAV-assisted file dispatching in a large-scale network. To this end, we apply NOMA in the multicast service of the file dispatching from the UAV to the GUEs. Besides, the UAV divides the data files into different file blocks (FBs) so that the GUEs can share their received FBs using D2D communications to reduce the transmission load of the UAV and improve the network performance. In the D2D-enhanced UAV-NOMA network, spatial reuse-based resource sharing between the NOMA links and the D2D links is allowed under centralized management. Hence, the network has a dynamic topology since the D2D links are established based on the GUEs' received FBs after the NOMA transmission. The interference environment is complicated because of the co-existence of the intragroup interference caused by NOMA and the intergroup interference caused by dynamic resource reuse. At the same time, the optimization problem is also complicated due to the overlap of the UAV's flying time, the NOMA transmission time, and the D2D transmission time. In order to solve the mission latency minimization problem, we propose a graph-based file dispatching (GFD) protocol in our investigated D2D-enhanced UAV-NOMA network by dividing the problem into three subproblems. First, we optimize the UAV's trajectory to make the path of the UAV that traverses the whole studied area as short as possible while ensuring the coverage of all the GUEs. Afterward, when the UAV flies over each coverage area, the UAV dispatches FBs with the help of NOMA. In this part, we use the graph theory to group NOMA users and allocate transmit power in order to maximize the efficiency of the UAV file dispatching. Finally, the GUEs that have received complete FBs are allowed to share their FBs using D2D via the same resources used by the NOMA links. The simulation results verify the efficiency of our proposed GFD protocol. The main contributions are summarized as follows.

- 1) For the first time, we propose to effectively combine NOMA and D2D file sharing together to support the UAV-assisted file dispatching in a large-scale network, in order to minimize the mission latency and improve the network performance. In such a system, the UAV flies over the entire studied area to cover all the GUEs and uses NOMA to dispatch FBs to the GUEs, while the GUEs with different FBs can share their FBs via the same resources at the same time.
- 2) In order to efficiently deal with the dynamic network topology, the complicated interference environment, and the working time overlap, we decompose the optimization problem into three subproblems and propose a novel and efficient GFD protocol to solve them.
- 3) In the proposed GFD protocol, the UAV's trajectory and the NOMA user groups are optimized reasonably, and the interference between the NOMA links and the D2D links is well controlled by graph-based algorithms. As a consequence, the UAV's efficiency in accomplishing the file dispatching mission is well improved.

The remainder of this article is organized as follows. Section II introduces the related works. In Section III, the system model of the proposed D2D-enhanced UAV-NOMA networks and the problem formulation are presented. Section IV gives the details of the proposed GFD protocol. In Section V, the simulation methods, features, and results are introduced and evaluated. We finally conclude this article in Section VI.

#### II. RELATED WORK

In UAV-assisted communications, UAV deployment is a major issue. In the literature, the problems of UAV deployment have been studied from different perspectives. Alzenad *et al.* [24] proposed a 3-D placement scheme for the UAVs being applied as base stations (BSs), to maximize the coverage of the GUEs with different Quality-of-Service (QoS) requirements. Mozaffari *et al.* [25] proposed a UAV deployment scheme to provide mobile wireless communications, when the UAVs are utilized as BSs. Wang *et al.* [26] proposed an adaptive deployment scheme for a UAV-aided communication network, where the UAV serves randomly moving users' instantaneous traffic in the target cell.

In practice, the UAVs are not always stationary and they need to move according to different missions. Thus, the trajectory of the UAV needs to be designed in order to minimize the cost of completing the mission. Zeng *et al.* [27] investigated the trajectory optimization problem in UAV communication systems. They compared the performance of four trajectory optimization schemes on the completion time of broadcasting and obtained an optimized trajectory design that makes

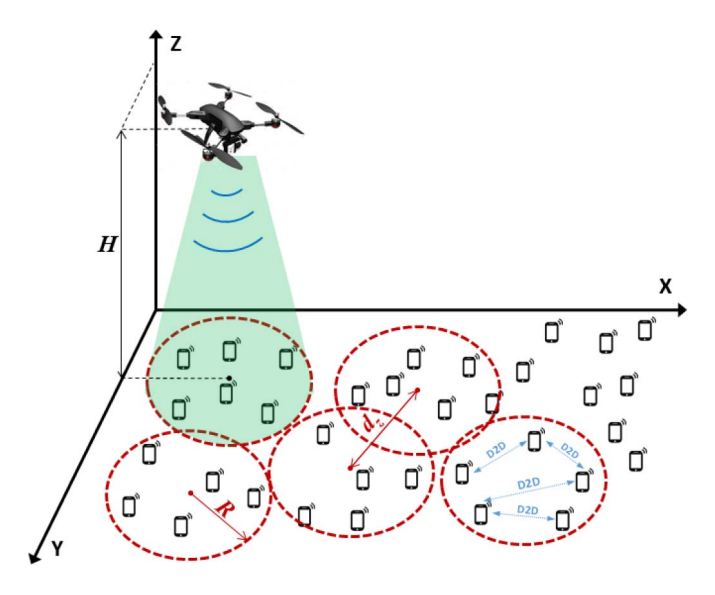


Fig. 1. Illustrated D2D-enhanced UAV-NOMA network.

the UAV take a short time duration to complete the mission. The energy efficiency maximization problem of the fixed-wing UAVs was studied in [28] and [29], through the joint design of the UAV's trajectory and transmit power. Besides, a UAV can also be used as a relay to support communications. Zhang *et al.* [30] studied a multihop relay system with multiple UAVs as relays and they maximized the network throughput by jointly optimizing the trajectories and transmit power.

Recently, the combination of NOMA and UAV-assisted communications has attracted a lot of attention, and the related issues have also been studied in the literature. Zhao *et al.* [31] studied the problem of maximizing the sum rate of UAV-assisted NOMA networks through an optimized trajectory of the UAV and precoding vectors of the NOMA BS. In [32], the UAV's placement issue was studied with the aid of machine learning techniques in the UAV-NOMA networks, where three case studies were presented. Sohail *et al.* [33] investigated the sum-rate maximization problem with reduced energy consumption and proposed a methodology to maximize NOMA performance in the UAV-assisted communication systems.

#### III. SYSTEM MODEL AND PROBLEM FORMULATION

# A. System Description

As illustrated in Fig. 1, we consider a typical UAV-assisted communication system with M GUEs denoted by  $\mathcal{M}$ . All the GUEs request for receiving the same data file with the size of W bits, which may be an image tile for a map or a video, etc. A rectangular coordinate system is established in a specific area to contain all the GUEs and the location of GUE  $m \in \mathcal{M}$  within the region is denoted by  $\mathbf{w}_m \in \mathbb{R}^{2\times 1}$ . In this article, we assume that the GUEs do not move quickly, which means that the GUEs are relatively in a quasistatic manner on the ground. In practice, the GUE can be a sensor node, a military installation, a traffic facility, or some other intelligent devices that are fixed somewhere and have the request for data files. For example, the target users/nodes of military installations that are scattered in the mountains or places have just

experienced disasters may not have the facilitation to access to the Internet. These installations generally do not have the ability to move arbitrarily. The GUEs' locations are collected by the UAV through information feedback. In the investigated scenario, one UAV behaves as the transmitter flying over the considered region while dispatching the requested data file. The altitude of the UAV is fixed to H. Note that the terrain and signal coverage should be taken into account when a specific UAV's altitude is set. Generally, a higher altitude leads to a larger signal coverage but an increased corresponding largescale fading. On the contrary, a reduced UAV's altitude may lead to a better channel gain but the ability to cope with complex terrain will decline [34]. Assume that the UAV uses a directional antenna, and thus the projection of the beam onto the ground is a circle, which is highlighted by the red dashed circle in Fig. 1. The circle with radius R represents the signal coverage of the UAV. The set of Z coverage circles is denoted by  $\mathcal{Z}$ , in which all the GUEs should have a guaranteed QoS.  $d_z$ is the distance between two circle centers. The UAV's trajectory projected onto the ground with respect to time t is denoted by  $\mathbf{q}(t) \in \mathbb{R}^{2 \times 1}$ , and the horizontal flying speed is v m/s.

In our proposed UAV-NOMA system, the UAV dispatches files to the GUEs within its current coverage to support multicast services with the help of NOMA. Two phases are contained in the network, that is, the NOMA phase in which the UAV dispatches files using NOMA and the D2D phase in which the GUEs exchange their files. Specifically, when files are dispatched through NOMA, the files can be divided into F different FBs, denoted by  $\mathcal{F}$ , and distributed to different GUEs using NOMA in the NOMA phase. After that, the GUEs that have different FBs can form U D2D pairs, denoted by U, and share FBs with each other in the D2D phase in order to improve the overall efficiency of file dispatching and reduce the total mission latency  $T_{\text{total}}$  of the UAV. C RBs, denoted by C, are allocated appropriately to different communication links. Therefore, in addition to optimizing the UAV's trajectory, the communication phase (i.e., the NOMA phase and the D2D phase) switching/coexisting issue should be effectively scheduled and the RBs should be allocated reasonably to avoid strong interference and reduce the failure probability of file transmission.

# B. Successive Interference Cancellation

Similar to code-division multiple access (CDMA) communication systems, the introduction of overlapped information at the transmitter not only improves the spectral efficiency but also brings the problem of multiple access interference (MAI). In NOMA communication systems, orthogonal frequency-division multiplexing (OFDM) technology can still be utilized for subchannel transmission. The subchannels are orthogonal with each other without any interference. However, a subchannel can be shared by multiple users in NOMA, which will result in MAI. As for the MAI elimination problem, plenty of achievements have been made in the research process of the third-generation (3G) mobile communication systems. The SIC is one of the effective technologies to eliminate the MAI [35], [36]. With NOMA, different signal power

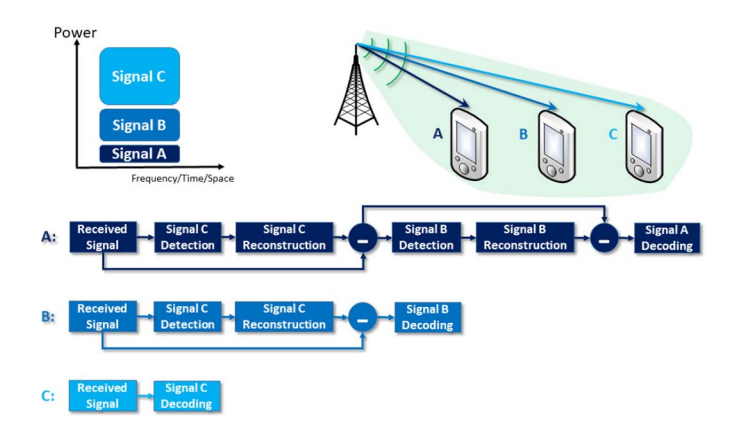


Fig. 2. NOMA with successive interference cancellation.

is allocated to different users based on their channel state information (CSI) to distinguish the users on the same sub-channel. Then, NOMA receivers use SIC to realize multiuser detection.

The basic principle of SIC is to subtract the interference generated by the signal with a higher allocated power level step by step. The SIC receiver makes multiple-user detection one by one in the received signal. When a user is detected, the MAI caused by this user's signal is subtracted at the same time. The detection is operated according to the order of signal power, which means that the signal with the maximum power is detected first. This detection and eliminating cyclic operation will keep working until all MAI is eliminated.

In a typical NOMA system, as shown in Fig. 2, the BS sends superimposed messages to the users with different power. User A has the shortest distance to the BS, which means it has the best channel condition compared with the other users, whereas user C has the worst channel condition. To make sure all the users can decode their own messages successfully, the BS needs to allocate transmit power in the order of C > B > A. Then, user C can decode its own message immediately by regarding the other users' messages as the noise. User B has to first decode user C's message and then subtract it from its received signal to get user B's own message, whereas user A has to decode both user B's and A's messages before decoding its own message, which shows that the more users participate in NOMA, the more complex the receiver is. Therefore, the number of NOMA users cannot be increased blindly to avoid excessive processing delay for the users with the best channel condition.

# C. Channel Analysis

In our investigated D2D-enhanced UAV-NOMA system, there are two main types of communication links, that is, the UAV-GUE link and the D2D link. Correspondingly, we have to consider two different channel models.

1) UAV-GUE Link: Denote  $\mathcal{H}_m$  as the channel coefficient between the UAV and GUE m, which can be given as

$$\mathcal{H}_m = \sqrt{\beta_m} g_m \tag{1}$$

where  $\beta_m$  denotes the path loss and  $g_m$  is the fading coefficient. The path loss usually depends on the distance

which can be given as

$$\beta_m = \beta_0 d_m^{-\alpha} \tag{2}$$

where  $\beta_0$  denotes the channel power gain at a unit distance,  $\alpha$  denotes the path-loss factor, and  $d_m$  is the distance between the UAV and GUE m at time t, which can be given as

$$d_m = \sqrt{\|\mathbf{q}(t) - \mathbf{w}_m\|^2 + H^2}.$$
 (3)

As for the fading coefficient  $g_m$ , it usually contains shadowing and various small-scale fading. Typically, the UAV-GUE links consist of a LoS link and a large number of independent links, so the channel can be characterized as a Rician fading model [27], [37]. Thus, we have

$$g_m = \sqrt{\frac{\kappa_m}{\kappa_m + 1}} g_m^{\text{main}} + \sqrt{\frac{1}{\kappa_m + 1}} g_m^{\text{scatter}}$$
(4)

where the first item corresponds to the LoS link arriving with uniform phase, and the second item corresponds to the aggregation of all the reflective and scattering links, independent of the LoS link.  $\kappa_m$  denotes the Racian factor, which is the ratio of the energy in the LoS link to the energy in the scattering links. The greater the  $\kappa_m$  is, the stronger certainty the channel is.  $g_m^{\text{main}}$  is the channel component of LoS link with  $|g_m^{\text{main}}| = 1 \cdot g_m^{\text{scatter}}$  denotes the channel component of the scattering link, which is a circular symmetric complex Gaussian random variable with  $g_m^{\text{scatter}} \sim \mathcal{CN}(0, \sigma^2)$  [38].

2) D2D Link: Denote  $\mathcal{H}_u$  as the channel coefficient between the GUEs in D2D pair  $u \in \mathcal{U}$ . The GUEs in one D2D pair may also have a LoS link between them, and thus the channel of D2D links can be characterized as a Rician fading model as well. Then, we have

$$\mathcal{H}_{u} = \sqrt{\beta_{u}} g_{u}$$

$$= \sqrt{\beta_{0} d_{u}^{-\alpha}} \left\{ \sqrt{\frac{\kappa_{u}}{\kappa_{u} + 1}} g_{u}^{\text{main}} + \sqrt{\frac{1}{\kappa_{u} + 1}} g_{u}^{\text{scatter}} \right\}$$
(5)

where  $\beta_u$  denotes the path loss,  $g_u$  denotes the fading coefficient,  $d_u$  denotes the distance between GUE  $u_1 \in \mathcal{U}$  and  $u_2 \in \mathcal{U}$  in D2D pair u, and  $\kappa_u$  denotes the Racian factor.  $g_u^{\text{main}}$  is the channel component of the LoS link with  $|g_u^{\text{main}}| = 1$ , and  $g_u^{\text{scatter}}$  is the channel component of the scattering link with  $g_u^{\text{scatter}} \sim \mathcal{CN}(0, \sigma^2)$ .  $d_u$  is given by

$$d_u = \|\mathbf{w}_{u1} - \mathbf{w}_{u2}\| \tag{6}$$

where  $\mathbf{w}_{u1}$  and  $\mathbf{w}_{u2}$  are the locations of the two GUEs in D2D pair u.

# D. Problem Formulation

Generally, the number of GUEs included in one NOMA group is random. A fixed number of GUEs in one NOMA group can limit the multiuser interference within the NOMA group and reduce the computational complexity. The

set of E NOMA groups is denoted by  $\mathcal{E}$ , and we assume that there are O GUEs in each NOMA communication group. Note that  $M = Q \times E$ . The UAV flies over the whole area for file dispatching. In each coverage area, the UAV dynamically chooses GUEs (based on the NOMA principle) to set up NOMA groups and sends different FBs with different power to the GUEs. Meanwhile, the GUEs can share different FBs using D2D via appropriate RB to minimize total mission latency  $T_{\text{total}}$ . As a result, the investigated problem can be divided into three parts.

- 1) The first part is to optimize the UAV's trajectory to make the UAV's flight distance as short as possible. The flying time of the UAV has a great affect on  $T_{\text{total}}$  because the UAV's flying speed is limited. Therefore, it is very important to optimize the UAV's trajectory reasonably.
- 2) The second part is to form NOMA groups carefully when the UAV is dispatching FBs in each coverage area. With appropriate management, NOMA can significantly improve the spectral efficiency, support more GUE connections, and reduce the latency.
- 3) The last part is to schedule the NOMA phase and the D2D phase and make sure that the two phases do not cause too much interference while resource sharing.
- 1) UAV Trajectory Optimization: The center of each UAV's coverage area, that is, the spot where the UAV can hover at, can be regarded as an MBS point (MBSP). The UAV has to cover as many GUEs as possible at each MBSP with the coverage radius R. The UAV can dispatch files during the flight or when hovering at each MBSP. However, the UAV needs to fly over all the Z MBSPs. Hence, our objective here is to determine the locations of MBSPs reasonably and then schedule the visiting order so as to minimize the total flying time  $t_f$ . The flying time minimization problem can be expressed as

$$(G1): \min \ t_f = \sum_{z \in \mathcal{Z}} \frac{d_z}{v} \tag{7a}$$

$$\|\mathbf{w}_{m}^{z} - \mathbf{w}_{z}\| \le R \quad \forall z \in \mathcal{Z}$$
 (7b)

where  $d_z$  denotes the distance between two MBSPs, given by  $\|\mathbf{w}_{z1} - \mathbf{w}_{z2}\|$ ,  $\mathbf{w}_z \in \mathbb{R}^{2 \times 1}$  denotes the location of the MBSP in coverage  $z \in \mathcal{Z}$ , and  $\mathbf{w}_m^z \in \mathbb{R}^{2 \times 1}$  denotes the location of the GUE within z. Equation (7b) ensures that all the GUEs are traversed by the UAV.

2) NOMA Group Construction: In our investigated scenario, the main task of the UAV is to dispatch data files. We divide W bits file into F FBs and dispatch the FBs to Q GUEs using NOMA so that the advantages brought by NOMA can be made full use of. Note that  $Q \ge F$ . In the NOMA group  $e \in \mathcal{E}$ , the received signal on RB  $c \in \mathcal{C}$  at user  $m_q \in \mathcal{M}$  $(q = 1, 2, \dots, Q)$  can be expressed as

$$y_{m_q}^e = \sum_{i=1}^{Q} \mathcal{H}_{m_q} \sqrt{a_{m_i}^e P_e} x_{m_i} + \sum_{u \in \mathcal{U}} \eta_e^u \mathcal{H}_{u_q} \sqrt{P_u} x_u + \zeta_{m_q}$$
 (8)

where  $\mathcal{H}_{m_q}$  and  $\mathcal{H}_{u_q}$  denote the channel gains from the UAV and the transmitter of D2D pair  $u \in \mathcal{U}$  to the GUE  $m_q$ , respectively, which are given in Section III-C.  $a_{m_i}^e$  denotes the transmit power allocation coefficient of NOMA with  $0 < a_{m_i}^e < 1$ .  $P_e$  and  $P_u$  denote the total transmit power allocated by the UAV to each NOMA group and the GUE's transmit power, respectively.  $x_{m_i}$  and  $x_u$  denote the transmit signals from the UAV and D2D pair u, respectively.  $\zeta_{m_a}$  is the additive white Gaussian noise (AWGN) with variance  $\sigma^2$ . The RB allocation indicator is denoted by  $\eta_e^u$ .  $\eta_e^u = 1$  when e and u are working through the same RB simultaneously, otherwise,

Therefore, the received SINR at  $m_q$  can be given as

$$\varphi_{m_q} = \frac{|\mathcal{H}_{m_q}|^2 P_e a_{m_q}^e}{I_{m_q} + I_{u_q} + \sigma^2} \tag{9}$$

where  $I_{m_q}$  and  $I_{u_q}$  denote the interference caused by the superposition signals of NOMA and the interference caused by the resource reusing by D2D pairs, respectively.

Assume that Q GUEs in the NOMA group e are sorted in the increasing order of  $d_m$ , that is,  $d_{m_1} < d_{m_2} < \cdots < d_{m_O}$ . Then, the interference can be expressed as

$$I_{m_q} = P_e \left| \mathcal{H}_{m_q} \right|^2 \sum_{i=1}^{q-1} a_{m_i}^e \tag{10}$$

$$I_{u_q} = \sum_{u \in \mathcal{U}} \eta_e^u |\mathcal{H}_{u_q}|^2 P_u. \tag{11}$$

Based on (9) and the Shannon formula, we can obtain the transmission rate of  $m_q$  as

$$\mathfrak{R}_{m_a} = \mathrm{BW}_e \cdot \log_2(1 + \varphi_{m_a}) \tag{12}$$

where BW<sub>e</sub> denotes the bandwidth allocated by the UAV to the NOMA group e.

Therefore, the objective in this part is to maximize the minimum rate of all the UAV-GUE links, and thus reduce the time of the UAV's file dispatching, which can be expressed as

$$(G2): \max \min \left\{ \mathfrak{R}_{m_a} \right\} \tag{13a}$$

s.t. 
$$\sum_{q=1}^{Q} a_{m_q}^e = 1 \quad \forall e \in \mathcal{E}$$
 (13b)

$$\sum_{e \in \mathcal{E}} P_e \le P_{uav} \tag{13c}$$

$$Q \ge F \tag{13d}$$

$$Q \ge F$$
 (13d)

$$\varphi_m \ge \varphi_0 \quad \forall m \in \mathcal{M}$$
(13e)

where (13b) limits the total power allocated to the GUEs within each NOMA group to  $P_e$ , (13c) limits the total power allocated to all the NOMA groups to  $P_{uav}$ , and (13d) ensures that all the FBs are available within each NOMA group.  $\varphi_m$ denotes the SINR received by GUE  $m \in \mathcal{M}$ . Equation (13e) ensures that the received SINR at each GUE is greater than the demodulation threshold  $\varphi_0$ .

3) Phase Switching Control: When receiving a complete FB, the GUEs with different FBs can be chosen to work in the D2D phase for file sharing. In order to improve the spectral efficiency, D2D links are allowed to reuse the RBs used by NOMA links. It is vital to ensure that no substantial interference exists between D2D and NOMA links, and thus an efficient interference control and resource allocation scheme is necessary. In addition, priority should be given to the NOMA transmission when inevitable strong interference between D2D and NOMA links exists.

When the received SINR at NOMA users is analyzed, the influence of D2D links has been already taken into account as shown in (8). Correspondingly, when the GUEs are working in the D2D phase, the signal  $y_u$  and the SINR  $\varphi_u$  received by the receiver in D2D pair u are given by

$$y_{u} = \mathcal{H}_{u}\sqrt{P_{u}}x_{u} + \sum_{e \in \mathcal{E}} \sum_{i=1}^{Q} \eta_{e}^{u} \mathcal{H}_{u}\sqrt{a_{m_{i}}^{e} P_{e}}x_{m_{i}} + \sum_{u' \in \mathcal{U}} \eta_{e}^{u'} \mathcal{H}_{u'}\sqrt{P_{u'}}x_{u'} + \zeta_{u}$$
(14)

$$\varphi_u = \frac{|\mathcal{H}_u|^2 P_u}{I_{u'} + I_e + \sigma^2} \tag{15}$$

where  $\mathcal{H}_{u'}$  denotes the channel gain from the transmitter of D2D pair  $u' \in \mathcal{U}$  ( $u' \neq u$ ) to the receiver of D2D pair u,  $P_{u'}$  denotes the transmit power of u',  $x_{u'}$  denotes the transmit signal in D2D pair u', and  $\zeta_u$  is the AWGN with variance  $\sigma^2$ .  $\eta_e^{u'}$  is the RB allocation indicator with the same meaning of  $\eta_e^u$ , that is,  $\eta_e^{u'} = 1$  when e and u' are working through the same RB simultaneously, otherwise,  $\eta_e^{u'} = 0$ . The interference caused by the resource reusing with other D2D pairs  $(I_{u'})$  and NOMA groups  $(I_e)$  can be expressed as

$$I_{u'} = P_{u'} \cdot \sum_{u' \in \mathcal{U}, u' \neq u} \eta_e^{u'} |\mathcal{H}_{u'}|^2$$
 (16)

$$I_e = \sum_{e \in \mathcal{E}} \eta_e^u |\mathcal{H}_u|^2 P_e. \tag{17}$$

Then, the transmission rate of D2D pair u can be expressed as

$$\Re_u = BW_u \cdot \log_2(1 + \varphi_u) \tag{18}$$

where  $BW_u$  denotes the bandwidth allocated to D2D pair u. Therefore, the objective here is to maximize the minimum rate of all the D2D pairs, which can be given as

$$(G3): \max \min \{\mathfrak{R}_u\} \tag{19a}$$

s.t. 
$$\varphi_u > \varphi_0 \quad \forall u \in \mathcal{U}$$
 (19b)

s.t. 
$$\varphi_u \ge \varphi_0 \quad \forall u \in \mathcal{U}$$
 (19b)
$$\sum_{e \in \mathcal{C}} \eta_e^u \le 1 \quad \forall e \in \mathcal{E}, u \in \mathcal{U}$$
 (19c)

$$\sum_{e,u} \eta_e^u \le \rho \quad \forall c \in \mathcal{C} \tag{19d}$$

where (19b) guarantees each GUE working in the D2D phase to have a required OoS. Equation (19c) limits the number of RBs allocated to each communication group to 1. Equation (19d) restricts the amount of communication links that can reuse the same RB at the same time to  $\rho$  so as to ensure that each communication link in the same RB can obtain a required QoS.

The time of NOMA transmission  $t_N^z$  and D2D transmission  $t_D^z$  can be expressed as

$$t_N^z = \frac{W}{F \cdot \min\{\mathfrak{R}_{m_a}\}} \tag{20}$$

$$t_D^z = \frac{W}{F \cdot \min\{\Re_u\}}.$$
 (21)

Therefore, the ultimate objective based on the above analysis can be given as

$$(G): \min \qquad T_{\text{total}} = \sum_{z \in \mathcal{Z}} \max \left\{ t_f^z, t_N^z \right\} \quad (22a)$$

$$\text{s.t. } \sum_{z \in \mathcal{Z}} t_D^z \le T_{total} \quad (7b)$$

$$(13b)-(13e)$$

$$(19b)-(19d). \quad (22b)$$

Note that FBs can be dispatched/shared when the UAV is flying or hovering. In our proposed scenario, the NOMA phase and the D2D phase are working simultaneously during the UAV's flight. Thus, in problem G, if the time of file transmission is less than that of the UAV's flight between different coverage circles, the UAV will fly at its maximum speed. In this case, what needs to be optimized is the file transmission rate so that the NOMA transmission will take as short time as possible. On the contrary, if the time of file transmission is more than that of the UAV's flight between different coverage circles, the UAV has to reduce its flying speed to ensure file transmission. In this case, the UAV's flying time is the determinant of  $T_{\text{total}}$ . Equation (22b) ensures that the D2D phase can be completed before the UAV completes its flight. For convenience, the notations used throughout this article are summarized in Table I.

#### IV. GRAPH-BASED FILE DISPATCHING PROTOCOL

In order to solve the resource allocation problems in our proposed UAV-NOMA scenario, and to enable the UAV to complete the file dispatching mission with the shortest time, we propose a GFD protocol in this section. In the GFD protocol, the UAV should first determine the locations of MBSPs to cover all the GUEs in the whole area with the minimum number of MBSPs, then plan the path traversing all the MBSPs to minimize the total flying distance. After that, the UAV will fly sequentially to each of the MBSPs along the planned path to dispatch FBs using NOMA (the NOMA phase). The GUEs with different FBs will start to share FBs after receiving FBs (the D2D phase). Similar to the problem formulation, the GFD protocol will be described in three parts in the following and the flowchart of the GFD protocol is provided in Fig. 3.

#### A. UAV Trajectory Optimization

1) MBSP Location Determination: With a given area that contains M GUEs, the first step of solving the problem G1 is to find the appropriate locations of the MBSPs, so as to minimize the total number of MBSPs and ensure that each GUE is covered by at least one MBSP. The location determination problem of the MBSPs is a typical geometric disk cover one [39] and we solve this problem by applying the spiral MBS placement (SMBSP) algorithm proposed in [40].

First, all the outermost GUEs are categorized as boundary GUEs  $\mathcal{GUE}_{bo}$  and arranged in counterclockwise order. The rest of the GUEs that are not on the boundary naturally become inner GUEs  $\mathcal{GUE}_{in}$ . A boundary GUE  $m_{bo} \in \mathcal{GUE}_{bo}$  is randomly selected as the first MBSP z at the beginning. Next,

TABLE I SUMMARY OF NOTATIONS

	Symbol	Meaning		Symbol	Meaning
UAV	$\mathbf{q}(t) \in \mathbb{R}^{2 \times 1}$	Trajectory	D2D u	$\zeta_u$	AWGN
	H	Altitude		$BW_u$	Bandwidth allocated to the D2D pair u
	v	Horizontal flight speed		$y_u$	Received signal at the receiver of D2D pair u
	$d_c$	Distance between two coverage circle centers		$x_u, x_{u'}$	Transmitting signal from the transmitter of D2D pair $u, u'$
	$P_{UAV}$	Total transmit power of the UAV		$P_u, P_{u'}$	Transmit power of the transmitter of D2D pair $u, u'$
	$t_f$	Total flying time		$\varphi_u$	Received SINR at the receiver of D2D pair $u$
MBS	$\mathcal{Z} = \{1, 2, \cdots, Z\}$	Set of MBSP's coverage circles	NOMA Group e	$I_{u'}, I_e$	Interference caused by the resource reusing by another D2D pair $u'$ , NOMA group $e$
z	$\mathbf{w}_z \in \mathbb{R}^{2  imes 1}$	Location		$\mathfrak{R}_u$	Transmission rate
	R	Radius of MBSP's coverage circle		$\mathcal{E} = \{1, 2, \cdots, E\}$	Set of NOMA groups
	$d_z$	Distance between two MBSPs		Q	Number of GUEs in one NOMA group
	$\mathcal{M} = \{1, 2, \cdots, M\}$	Set of GUEs		$m_q$	The qth GUE in one NOMA group
	$\mathbf{w}_m \in \mathbb{R}^{2  imes 1}$	Location		$\mathcal{H}_{m_q}, \mathcal{H}_{u_q}$	Channel coefficient from the UAV, the transmitter of D2D pair $u$ , to the GUE $m_q$
	$\mathbf{w}_m^z \in \mathbb{R}^{2 imes 1}$	Location of the GUE within z		$a_{m_i}^e$	Transmit power allocation coefficient
GUE	$d_m$	Distance between the UAV and GUE $m$		$P_e$	Transmit power allocated to one NOMA group
m	$\mathcal{H}_m$	Channel coefficient between the UAV and GUE $m$		$x_{m_i}$	Transmit signal
	$\beta_m$	Path loss		$y_{m_q}^e$	Received signal at GUE $m_q$
	$g_m$	Fading coefficient		$\varphi_{m_q}$	Received SINR at GUE $m_q$
	$g_m^{main}$	Channel component of LoS link		$\zeta_{m_q}$	AWGN
	$g_m^{scatter}$	Channel component of scattering link		$I_{m_q}, I_{u_q}$	Interference caused by the superposition signals with NOMA, resource reusing by D2D links
	$\kappa_m$	Racian factor		$BW_e$	Bandwidth allocated to the NOMA group e
	$\mathcal{U} = \{1, 2, \cdots, U\}$	Set of D2D pairs		$\mathfrak{R}_{m_q}$	Transmission rate
	$\mathbf{w}_{u1}, \mathbf{w}_{u1}$	Locations of the two GUEs in D2D pair $u$	Others	$\mathcal{F} = \{1, 2, \cdots, F\}$	File block
	$d_u$	Distance between the GUEs in D2D pair $\boldsymbol{u}$		$\mathcal{C} = \{1, 2, \cdots, C\}$	RB
D2D	$\mathcal{H}_u, \mathcal{H}_{u'}$	Channel coefficient of D2D link $u, u'$		α	Path loss factor
u	$\beta_u$	Path loss		$\beta_0$	Chaneel power gain at an unit distance
	$g_u$	Fading coefficient		$T_{total}$	Total time of mission completion
	$g_u^{main}$	Channel component of LoS link		W	Total file size in bits
	$g_u^{scatter}$	Channel component of scattering link		$\eta_e^u, \eta_e^{u'}$	RB allocation indicator
	$\kappa_u$	Racian factor		ρ	The maximum number of communication links that can reuse the same RB at the same time

the location of MBSP z is adjusted so that it can cover as many other boundary GUEs as possible while guaranteeing that GUE  $m_{bo}$  is covered. Then, the location of MBSP z will be adjusted again so as to cover the inner GUEs as many as possible on the premise of guaranteeing the currently covered boundary GUEs. Now, the first MBSP is located. After that, the new boundary GUEs are refound in all uncovered GUEs. The above processes are repeated until all the GUEs are covered. Finally, all the appropriate locations of MBSPs are obtained. The detailed operation of the SMBSP algorithm is summarized in Algorithm 1 with the complexity of  $\mathcal{O}(M^2 \log M)$ , and the derivations and detailed proof can be found in [40].

In Algorithm 1,  $\lambda$  denotes the set of uncovered GUEs and  $\mu$  denotes the initial boundary GUEs. In Algorithm 2,  $\mu_1$  denotes the initial boundary GUEs and  $\mu_2$  denotes the uncovered inner GUEs.

2) Flying Path Scheduling: After the locations of MBSPs are determined, the next step is to schedule the path of the UAV to fly over all the MBSPs, that is, the visiting order of all MBSPs so as to minimize the total flying distance. This problem can be modeled as a traveling salesman (TSM) problem, which is a classical NP-hard problem. The TSM problem is to find the minimum path of a traveler starting from a specific point, passing through all the given points, and finally returning to the original point. The most evident

# **Algorithm 1: SMBSP Algorithm**

```
Input: \mathcal{M}, R, \mathbf{w}_m.
Initialization: \lambda \leftarrow \mathcal{M}, \mathcal{Z} = \emptyset, i = 1.
while \lambda \neq \emptyset do
      Find all the boundary GUEs \mathcal{GUE}_{bo} arranged in
      counterclockwise order, and the inner GUEs \mathcal{GUE}_{in}.
      if i = 1 then
            Randomly select a boundary GUE m_{bo} as the first
           MBSP z. Let \mathbf{w}_z \leftarrow \mathbf{w}_{m_{bo}}.
      end
      Call [\mathbf{w}_z, \mu] = \mathbf{LocalCover}(\mathbf{w}_z, \{z\}, \mathcal{GUE}_{bo} - \{z\}).
      Let \mu_0 \leftarrow \mu.
      Call [\mathbf{w}_z, \mu] = \mathbf{LocalCover}(\mathbf{w}_z, \mu_0, \mathcal{GUE}_{in}).
      Let \lambda \leftarrow (\lambda - \mu), \mathcal{Z} \leftarrow \mathcal{Z} \cup \{z\}.
      Select the first uncovered boundary GUE m'_{bo}
      counterclockwisely next to m_{bo} from \mathcal{GUE}_{bo} - \mu_0.
     Let m_{bo} \leftarrow m'_{bo}, i \leftarrow (i+1).
end
```

algorithm is the exhaustive method, which is to find all the combinations and pick the shortest one. The permutation number of the exhaustive method is n! (where n is the number of nodes), which can be solved in  $\mathcal{O}(n^2 \cdot 2^n)$  time using dynamic programming. It also has many approximate solutions, such as

Output:  $\mathcal{Z}$ .

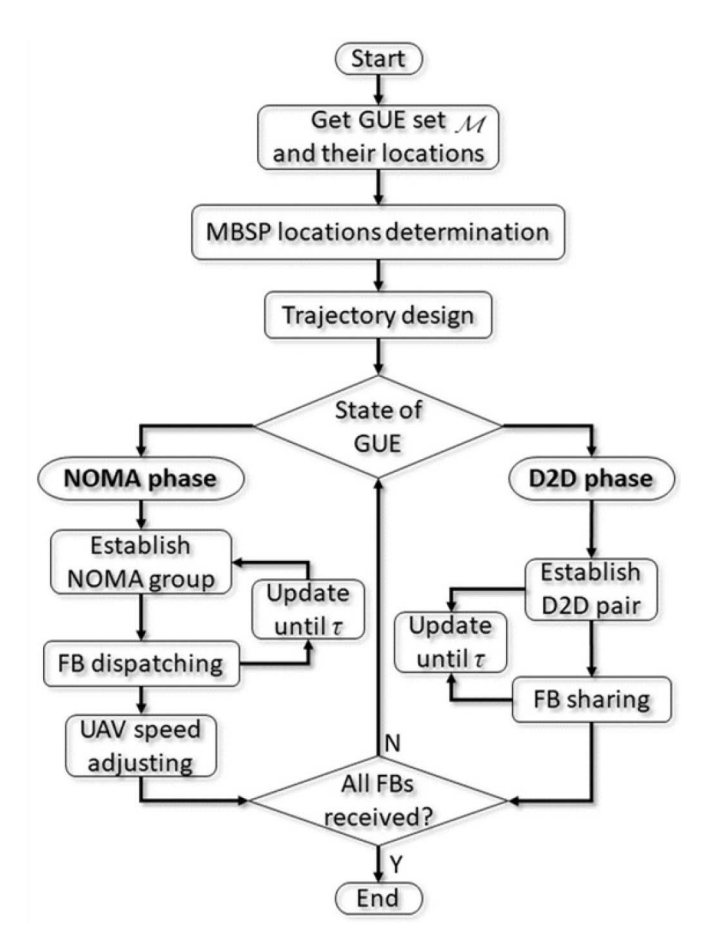


Fig. 3. Flow diagram of the GFD protocol.

# Algorithm 2: LocalCover Algorithm $[\mathbf{w}_z, \mu_1] = \mathbf{LocalCover}(\mathbf{w}_z, \mu_1, \mu_2)$ Input: $\mathbf{w}_z, \mu_1, \mu_2$ . while $\mu_2 \neq \emptyset$ do Update $\mu_2$ by excluding GUEs more than 2R away from any GUE in $\mu_1$ . Update $\mu_1$ ( $\mu_2$ ) by including (excluding) GUEs within distance R to z. Find GUE $m \in \mu_2$ with the shortest distance to z. **if** m can be covered by refining $\mathbf{w}_z$ via solving the 1-center problem then Add (remove) m to (from) $\mu_1$ ( $\mu_2$ ) else Stop. end end Output: $\mathbf{w}_z$ , $\mu_1$ .

the simulated annealing algorithm, greedy algorithm, genetic algorithm, ant colony algorithm, etc. [42], [43].

In this article, we apply the solver-based TSM (S-TSM) algorithm [41], which is a suboptimal method, to solve the TSM problem using binary integer programming. The main idea of the S-TSM algorithm is to solve an initial problem first to get the subtours of the solution. This transitional solution does not give one continuous path through all the

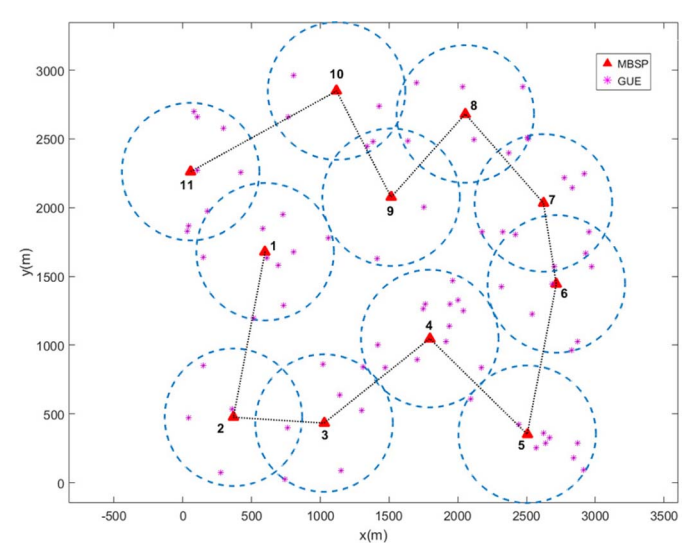


Fig. 4. Example of the optimized UAV trajectory.

points but instead has several disconnected loops. Then, an iterative process will be used to determine the subtours and add constraints until the subtours are eliminated. The detailed procedure of the S-TSM algorithm is given in [41] with the complexity of  $\mathcal{O}(Z^2)$ . An example of the optimized UAV trajectory is shown in Fig. 4.

In Fig. 4, the blue dashed circle denotes the coverage of each MBSP with a radius of *R*. The UAV will fly over the first MBSP to dispatch FBs to the GUEs within its coverage and then fly to the next MBSP sequentially. Finally, the UAV will fly to the starting MBSP when the whole area is traversed.

# B. NOMA Group Construction

After the optimization of the UAV's trajectory is completed, we focus on the efficiency of file dispatching when the UAV is flying over each MBSP in the problem G2. The UAV first divides all the GUEs within the coverage of  $z \in \mathcal{Z}$  into E NOMA groups based on their CSI when the UAV flies in coverage z. In the literature, a lot of efficient methods have been proposed for NOMA user grouping and power allocation [44]–[46]. In this article, we assume perfect SIC conditions, that is, the GUEs with better channel conditions can completely subtract the signals of the GUEs with weaker channel conditions. Then, we propose a suboptimal solution to solve the problem G2, which contains two steps. The GUEs are first divided into NOMA groups with a fixed power allocation coefficient and the next step is to refine the power allocation coefficient to further improve the performance.

1) NOMA User Grouping: In order to imitate the interference environment and form NOMA user groups, we apply the graph theory, which is widely used in wireless resource scheduling [47]–[49], to solve the problems. To solve the NOMA user grouping problem in G2, we propose a hypergraph-based grouping (HG-G) algorithm. The HG-G algorithm introduces the concept of hypergraph [18], [19].

Let  $\mathcal{HG} = (\mathcal{HV}, \mathcal{HE})$  be a hypergraph, where  $\mathcal{HV}$  is the set of vertices representing the GUEs within the coverage of z and  $\mathcal{HE}$  is the set of hyperedges representing the matching

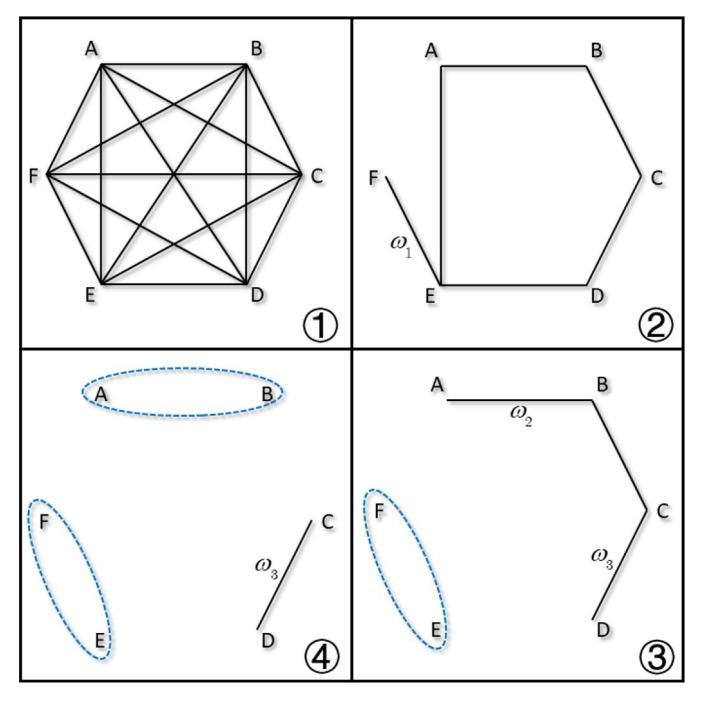


Fig. 5. Example of the HG-G algorithm with Q = 2.

relationships between vertices. Q GUEs are connected by hyperedge  $he \in \mathcal{HE}$  forming an NOMA group e. The weight  $\omega$  of hyperedge he is set to be the minimum SINR of Q GUEs in the NOMA group e. Here, the NOMA user grouping problem can be modeled as a valid matching in the weighted hypergraph  $\mathcal{HG}$ .

Definition 1: In a hypergraph  $\mathcal{HG} = (\mathcal{HV}, \mathcal{HE})$ , strongly delete a vertex  $vx \in \mathcal{HV}$  from  $\mathcal{HG}$  means removing all the hyperedges containing vx from  $\mathcal{HE}$  and then removing vx from  $\mathcal{HV}$ .

First, all the hyperedges are arranged in the descending order of their weights. Then, the hyperedge with the smallest weight is deleted sequentially until a vertex  $vx_1 \in \mathcal{HV}$  that connected by only one hyperedge  $he_1 \in \mathcal{HE}$  comes up. Thus, vertex  $vx_1$  and the other vertices contained in  $he_1$  form an NOMA group naturally.

Next,  $vx_1$  and the other vertices contained in  $he_1$  are strongly deleted from  $\mathcal{HG}$ . Then,  $vx_1$  and  $he_1$  are updated by finding the vertex again that connected by only one hyperedge. If more than one vertex meets the criterion, the hyperedge with the heaviest weight will be selected to be a new matching. The finding and deleting cyclic operation will be repeated until all the hyperedges in the hypergraph have been deleted.

Finally, the suboptimal NOMA groups satisfying problem G2 are obtained. Fig. 5 illustrates an example of the HG-G algorithm with Q=2. A hypergraph will degenerate into an ordinary graph when each hyperedge contains only two vertices. As we can see in Fig. 5①, the hypergraph (graph) is constructed with six users and the hyperedges (edges) represent the potential NOMA groups. Vertex F connected by only one edge appears, after all the edges with the minimum weight are deleted sequentially, which is shown in Fig. 5②. Then, we can make the decision that user F and E can form an NOMA group. The graph becomes what is shown in Fig. 5③

```
Algorithm 3: HG-G Algorithm
 Input: \mathcal{Z}, \mathbf{w}_m^z.
 Initialization: i \leftarrow 1.
 Construct hypergraph \mathcal{HG} = (\mathcal{HV}, \mathcal{HE}).
 \mathcal{HE}_{sort}=sort(\mathcal{HE}, 'descent').
 while \mathcal{HG} \neq \emptyset do
      Find the vertex vx_1 that connected by only one
      hyperedge he_1.
      while length(vx_1) = 0 do
       Delete the hyperedge with the smallest \omega
      if length(vx_1) > 1 then
           Find the vertex vx_1 with the biggest \omega.
           Update vx_1 and he_1.
      end
      if length(vx_1) = 1 then
           e_i \leftarrow e_i \cup he_1.
           Strongly delete vx_1.
           i \leftarrow i + 1.
      end
 end
 Output: \mathcal{E}.
```

when vertices F and E are strongly deleted. We can also see in Fig. 5③ that both vertices A and D are connected by only one edge. Assume that  $\omega_2 > \omega_3$ , and thus we choose vertices A and B to form an NOMA group leaving vertices C and D form an NOMA group naturally as shown in Fig. 5④.

The detailed procedure of the HG-G algorithm is summarized in Algorithm 3. Because of the double loop and the sorting process in the algorithm, the worst case complexity of the HG-G algorithm is  $\mathcal{O}(E^2)$ .

- 2) Power Allocation: Given the NOMA groups  $\mathcal{E}$ , power allocation optimization is performed within each NOMA group to further improve the performance of NOMA. Ali et al. [44] proposed an optimal transmit power and corresponding necessary conditions for NOMA transmission based on the minimum data rate requirement of NOMA users. For convenience, we name the algorithm proposed in [44] "OPA algorithm." In this article, we adopt the OPA algorithm to get a power allocation solution. Next, we find the smallest transmission rate  $\mathfrak{R}_{op}$  from the solution as the respective minimum rate requirement of the OPA algorithm. Then, we run the OPA algorithm again to get an improved smallest transmission rate  $\mathfrak{R}_{ne}$ . The iteration will be terminated until  $\mathfrak{R}_{ne} \mathfrak{R}_{op} \leq \epsilon$ , where  $\epsilon$  is a given stopping criterion. The power allocation algorithm is summarized in Algorithm 4.
- 3) Solution Updating (SU): The position relationship between the GUEs and the UAV will change along time because the UAV is flying continuously. Therefore, it will cause strong interference, if the solution of user grouping and power allocation is not adjusted. In order to solve the problem of relative position changing caused by the UAV's mobility, we set up a scheme updating mechanism, that is, the NOMA user grouping and power allocation schemes will be updated periodically after time interval  $\tau$ . Because the UAV's trajectory is preplanned and known, and the moving distance of the

### Algorithm 4: Power Allocation Algorithm

```
Input: \mathcal{E}, \mathbf{w}_m^z.

Initialization: Flag \leftarrow 1.

Run 'OPA' algorithm.

Find the smallest transmission rate \mathfrak{R}_{op}.

while Flag=1 do

Run 'OPA' algorithm with \mathfrak{R}_{op} as the respective minimum rate requirements.

Find the smallest transmission rate \mathfrak{R}_{ne}.

if \mathfrak{R}_{ne} - \mathfrak{R}_{op} \leq \epsilon then

| Flag \leftarrow 0.

end

end

Output: a_{m_i}^e, i = (1, 2, \cdots, Q).
```

UAV is limited in milliseconds, the periodic SU mechanism can well compensate for the mobility issue of the UAV.

## C. Phase Switching Control

Based on the GFD protocol proposed in the UAV-NOMA scenario, the D2D phase and the NOMA phase are working simultaneously. Hence, the file dispatching load of the UAV can be further reduced through D2D file sharing.

The GUEs will start to work in the D2D phase as long as they have finished FB receiving through NOMA. We use  $z \in \mathcal{Z}$  to represent the circle of the coverage of each MBSP as well. Then, the problem is to allocate RBs to D2D pairs in the same circle and determine which of the circles can reuse the same RB. To this end, we propose two alternatives in the following [i.e., the basic D2D scheme and the generalized D2D (GD2D) scheme].

1) Basic D2D Scheme: In this scheme, FBs are shared between every two GUEs. GUEs with different FBs are paired until all the GUEs get a whole data file. Here, we apply graph theory again.

We construct an ordinary graph  $\mathcal{G}=(\mathcal{V},\mathcal{ED})$  in which the vertices represent the GUEs and the edges represent that the two connected vertices have different FBs to share. The weight of each edge represents the transmission rate between the GUEs in each D2D pair without interference. Then, the edge with the heaviest weight is selected as the currently established D2D pair sequentially and the two vertices connected by this edge are strongly deleted from  $\mathcal{G}$ . After all the D2D pairs are selected, a round of FB sharing is completed. Then, a new graph is reconstructed based on the current condition and the above processes are repeated so that all the FBs can be shared.

In the D2D phase, different D2D pairs are allowed to share the same RB, that is, two D2D pairs  $u_1 \in \mathcal{U}$  and  $u_2 \in \mathcal{U}$  can share the same RB if the mutual interference between them is less than a threshold  $\Theta_{\varphi}$ . Different circles  $z_1 \in \mathcal{Z}$  and  $z_2 \in \mathcal{Z}$  can share RBs when the distance between the corresponding MBSPs is greater than a threshold  $\Theta_d > 2R$ . The proposed graph-based D2D pairing algorithm is provided in Algorithm 5.

2) Generalized D2D Scheme: This scheme is a terrestrial broadcasting scheme. In this scheme, all the GUEs with the

**Algorithm 5:** Graph-Based D2D Pairing Algorithm

```
Input: \mathcal{M}.
Initialization: Flag \leftarrow 1.
while Flag = 1 do
     Construct graph \mathcal{G} = (\mathcal{V}, \mathcal{ED}).
     Calculate the weight of each edge.
     while \mathcal{ED} \neq \emptyset do
         Find the edge ed with the largest weight.
         \mathcal{U} \leftarrow \{ed\}.
         Strongly delete the vertices connected by ed.
     end
     Call Algorithm 6.
     if No GUE needs FBs then
     | Flag \leftarrow 0
     end
end
Output: \mathcal{U}.
```

# Algorithm 6: RB Reusing Algorithm

```
Input: \mathcal{M}.

Initialization: Flag \leftarrow 1, \eta_e^u \leftarrow 0 (\forall u \in \mathcal{U}).

Construct graph \mathcal{G}' = (\mathcal{V}', \mathcal{ED}') in which the vertices represent D2D pairs and the edges represent the interference relationships.
```

Calculate the weight  $\omega'$  of each edge which means the interference between the D2D pairs.

```
\begin{array}{c|c} \textbf{for} \ u = 1 : U \ \textbf{do} \\ & \textbf{if} \ \omega_u' > \Theta_{\varphi} \ \textbf{then} \\ & | \ \eta_e^u \leftarrow 1 \\ & \textbf{end} \end{array}
```

**Output**:  $\mathcal{U}$ ,  $\eta_e^u(\forall u \in \mathcal{U})$ .

same FB in the same circle z form an FB group  $\aleph$ . The GUE within group  $\aleph$  that has the nearest average distance to the GUEs of other groups is selected to broadcast its FB so that only F GUEs work as the broadcasting transmitters at the same time to complete the FB sharing among GUEs within circle z. RBs are also allowed to be shared between different circles when the distance between the corresponding MBSPs is greater than the threshold  $\Theta_d$ .

Therefore, the problem here is to find the GUE in the group  $\aleph$  to broadcast its FB. Obviously, the most straightforward method is to select the most appropriate GUEs after calculating the distance between each two GUEs, which requires a large amount of computations. In order to reduce the processing complexity, we find the most appropriate GUEs in each FB group separately. First, the GUEs with FB<sub>1</sub> form a group  $\aleph_1$  and the remaining GUEs in z form another group  $\aleph_1$ . The GUEs within  $\overline{\aleph}_1$  form a polygon with its centroid VC<sub>1</sub>. Then, the GUE with the shortest distance to VC<sub>1</sub> in  $\aleph_1$  is picked to be the transmitter to share FB<sub>1</sub>. After that, the transmitters to share all the other FBs are picked in the same manner in turn. An illustration of this method is shown in Fig. 6 with F = 3.

3) Solution Updating: In practice, some of the scenarios in IoT may include mobile GUEs. Thus, the mobile GUEs

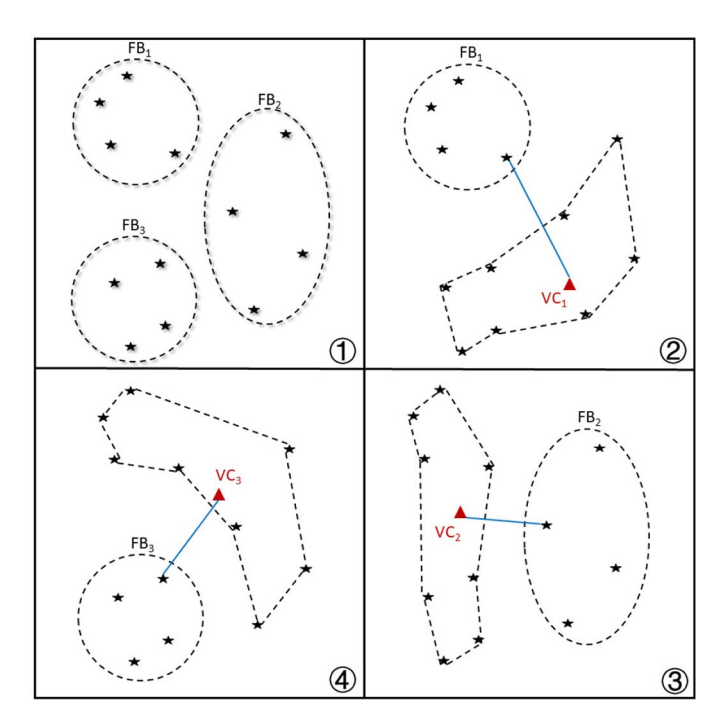


Fig. 6. Illustration of the GD2D scheme with F = 3.

are in danger of getting out of all the designed circles, which makes them unable to participate in the NOMA transmission. Specifically, it can be classified into two categories according to the GUEs' moving range during the whole mission.

- If the mobile GUEs are still in the predesigned circles that they belong to, the GUEs' movement can only affect the NOMA and D2D user grouping. Noticing this, the SU mechanism has already solved the corresponding problems.
- If some of the GUEs are out of their own circles, the GUEs that are not in any circle can still participate in the D2D phase to receive/share FBs.

Therefore, we set up an SU mechanism in the D2D phase as well. The D2D grouping will be updated periodically to make sure the GUEs that are out of circles can participate in the D2D transmission in time.

## V. NUMERICAL RESULTS AND DISCUSSION

Our simulation setup considers a 3 km×3 km square area covered by one UAV, and we randomly arrange M GUEs in the considered area on the ground. For simplicity and without loss of generality, we set Q = F = 2. As described in Section III-D, Q=2 means that each NOMA group has two receivers and F = 2 means that the data file with the size of W bits is divided into two FBs. Thus, the UAV can dispatch the two FBs to the two GUEs within the same NOMA group. Note that different values of Q and F can only affect the processing complexity of the receiver. A higher value of Q means more intragroup interference to the receivers, but at the same time it will further improve spectral efficiency. In our proposed HG-G algorithm, GUEs are grouped based on the same strict principle regardless of the value of Q. Thus, the system performance will not be greatly influenced by the value of Q. All the other parameters applied in our simulation are summarized in Table II.

TABLE II System Parameters

Parameters	Value	
Carrier frequency	2 GHz	
Total Bandwidth	1 MHz	
RB Bandwidth	10 KHz	
Path Loss Factor α	2.6	
Rician Factor	$\kappa_m = 2,  \kappa_u = 1.5$	
Reference Channel Gain $\beta_0$	−40 dB	
Noise Power $\sigma^2$	−109 dBm	
Noise Figure	10 dB	
UAV Transmit Power $P_{UAV}$	10 dBm	
UAV Speed v	50 m/s	
UAV Altitude H	100 m	
UAV Coverage Radius R	300 m	
GUE Transmit Power $P_u$	10 dBm	
File Size W	2 Mbits	
Updating Interval $ au$	1 ms	

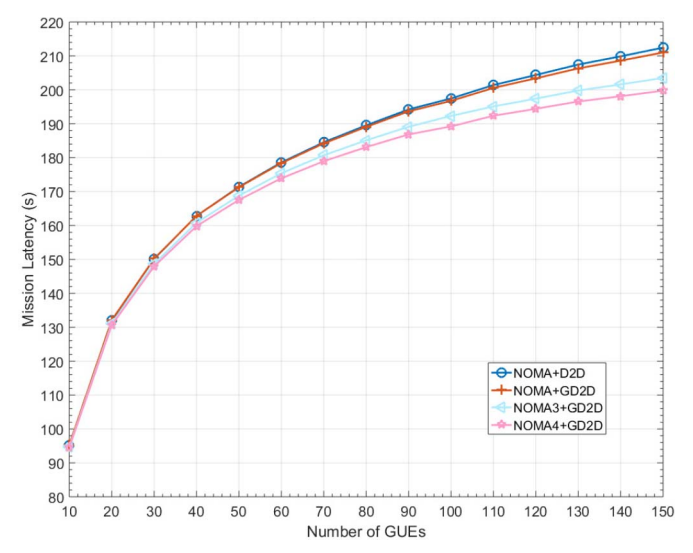


Fig. 7. Mission latency comparison when the UAV dispatches FBs during its flying.

In order to compare the file dispatching efficiency in different cases, we also include the situation that the UAV flies to the location of each MBSP and hovers for file dispatching. The D2D phase starts to work after the UAV completes the NOMA phase in one of the coverage circles, that is, the D2D phase is working when the UAV is flying between two MBSPs to avoid interference between the D2D phase and the NOMA phase, and utilize the UAV's flying time.

Given the coverage radius R and flying speed v of the UAV, the number of GUEs M affects the total mission latency  $T_{\text{total}}$ . Figs. 7 and 8 compare the total time for the UAV to complete the data file dispatching as the number of GUEs increases.

Fig. 7 shows  $T_{\text{total}}$  varies with M in case that the UAV dispatches FBs during its flying. As shown in Fig. 7, the mission latency of both NOMA+D2D and NOMA+GD2D schemes is increasing with the increase in the number of GUEs. This is because the increase in the number of GUEs leads to a widening range for the UAV to travel. On the other hand, it also increases the potential interference brought by resource reusing. When the number of GUEs further increases, the increasing rate of the total mission latency slows down. This is because the newly added GUEs can be directly assigned to the

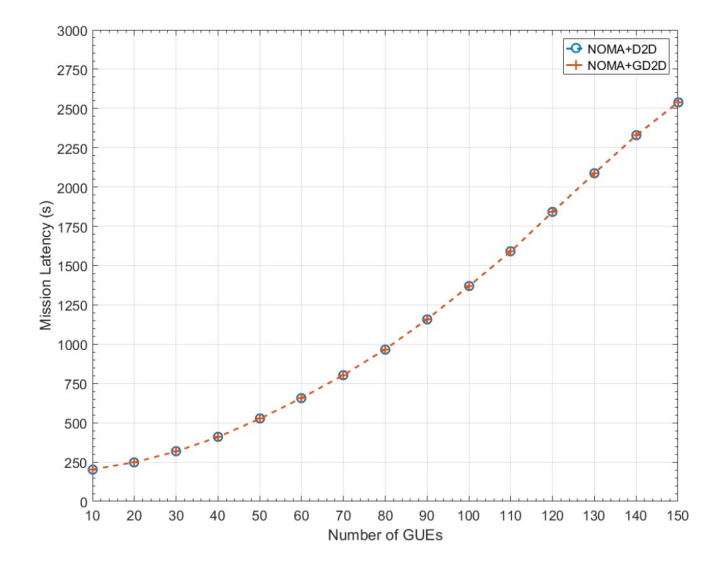


Fig. 8. Mission latency comparison when the UAV flies to the location of each MBSP and hovers for file dispatching.

existing coverage circles without replanning a new trajectory when the number of GUEs is large. We can also see that the performance of our proposed protocol with the NOMA+D2D scheme and the NOMA+GD2D scheme has only slightly difference. With the application of the NOMA+GD2D scheme, the total mission latency is a little less than that of the NOMA+D2D scheme. This is because the NOMA+GD2D scheme generates less interference to the NOMA users compared with the NOMA+D2D scheme, and thus the NOMA phase can complete FB transmission with less time. The system can choose which scheme to apply according to different requirements and situations. In addition, we also include the simulation when Q = F = 3 and Q = F = 4 (i.e., NOMA3+GD2D and NOMA4+GD2D in Fig. 7). As we can see, with more receivers contained in each NOMA group, it takes less time to dispatch the data file, which verifies that the application of NOMA can improve the performance and reduce the mission latency. However, it will lead to higher complexity and more interference at the receiver when the number of NOMA users increases. In practice, the UAV can determine the number of NOMA users based on the mission requirements.

Fig. 8 shows  $T_{\rm total}$  varies with M in case that the UAV first flies to the location of each MBSP and hovers for file dispatching, and then flies to the next MBSP. As we can see, in this case, the mission latency is much longer than that of the case that the UAV dispatches FBs during its flying. Although the frequent updates of resource allocation schemes are avoided, the flying time of the UAV between MBSPs is not effectively utilized, which results in longer time to complete the mission.

Fig. 9 shows the performance improvement of our proposed GFD protocol with D2D-enhanced UAV-NOMA communication architecture compared with other published schemes. Zeng *et al.* [27] listed three different schemes aiming at minimizing the total time consuming in the field of UAV-assisted file dispatching. Completion time minimization with strip-based waypoints (CTM-SW) indicates the strip-based scheme,

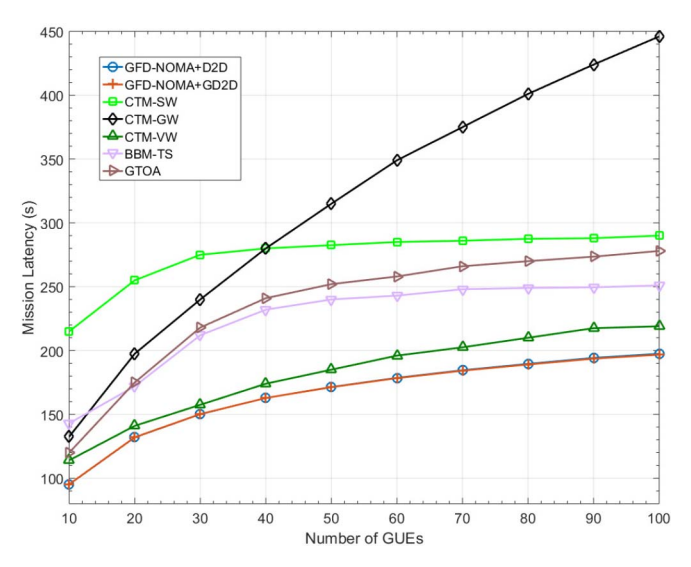


Fig. 9. Mission latency comparison with other schemes when the UAV dispatches FBs during its flying.

which programs the UAV to fly along predesigned rectangular strips that ensures full area coverage and to dispatch files through random linear network coding (RLNC). In completion time minimization with GUEs as waypoints (CTM-GW), the UAV has to fly over every GUE and dispatches files through RLNC. The scheme completion time minimization with virtual BSs as waypoints (CTM-VW) represents that the UAV is scheduled to fly over every center of the predesigned coverage circle and dispatches files through RLNC. Besides, we apply the branch-and-bound method (BBM) proposed in [50] with the TSM algorithm (i.e., BBM-TS). The group-based trajectory optimization algorithm (GTOA) proposed in [51] is also applied by setting the maximum radius of the transmission region as R. As we can see in Fig. 9, our proposed scheme has at most 10% performance improvement than the CTM-VW scheme.

As a baseline, we also employ different file dispatching schemes in the investigated scenario for UAV-assisted file dispatching. Figs. 10 and 11 compare the total time of the UAV to complete the data file dispatching as the number of GUEs increases with different file dispatching schemes.

Fig. 10 shows the case that the UAV dispatches FBs during its flying. In Fig. 10, the scheme "noNOMAnoD2D" represents that the UAV uses OFDMA to dispatch files and ensures that each GUE receives a complete data file. As we can see, the noNOMAnoD2D scheme is much less efficient than our proposed NOMA+D2D/GD2D scheme. Our proposed GFD protocol with NOMA+D2D/GD2D scheme will have more advantages especially when the number of the GUEs increases. The scheme "onlyNOMAnoD2D" represents that the UAV exploits NOMA to dispatch files without the assistance of D2D. In this case, the UAV has to send all FBs to each GUE through NOMA. Obviously, the onlyNO-MAnoD2D scheme takes less time than the noNOMAnoD2D scheme, due to the application of NOMA. However, because of the lack of D2D support, the flying time of the UAV between MBSPs is not fully utilized. Hence, the onlyNOMAnoD2D

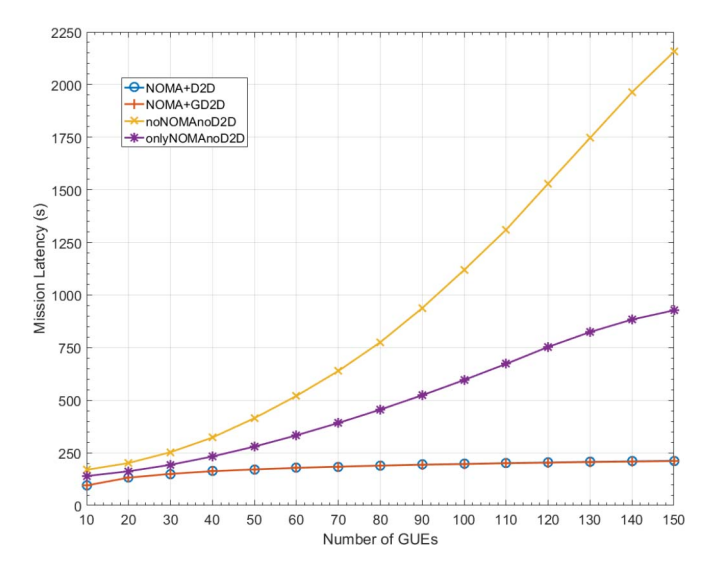


Fig. 10. Mission latency comparison with different schemes when the UAV dispatches FBs during its flying.

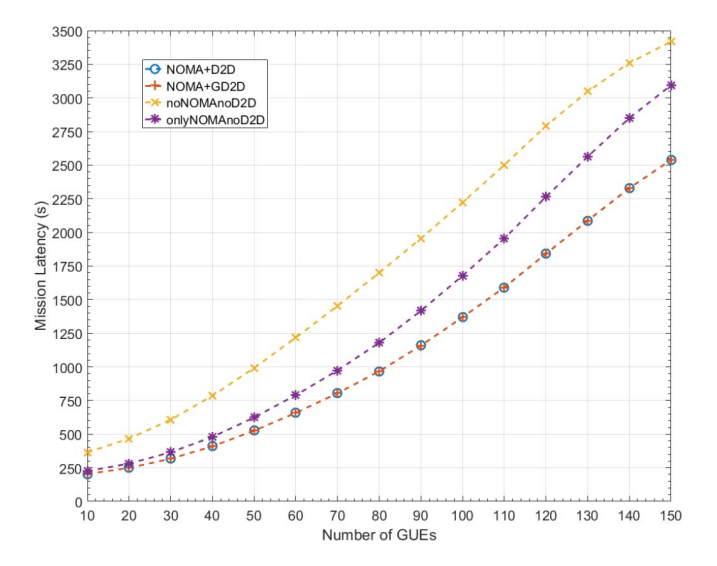


Fig. 11. Mission latency comparison with different schemes when the UAV flies to the location of each MBSP and hovers for file dispatching.

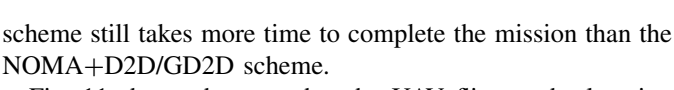


Fig. 11 shows the case that the UAV flies to the location of each MBSP and hovers for file dispatching. As we can see in Fig. 11, the mission latency of our proposed GFD protocol with the NOMA+D2D/GD2D scheme is about 30% shorter than that of the noNOMAnoD2D scheme and 20% shorter than that of the onlyNOMAnoD2D scheme.

Afterward, we analyze the influence of the UAV coverage radius R on the mission latency with M=80, which is shown in Figs. 12 and 13.

Fig. 12 shows the case that the UAV dispatches FBs during its flying. As we can see that the mission latency of our proposed GFD protocol with the NOMA+D2D/GD2D scheme first decreases and then increases with the increase of R. This is because the UAV can only cover a very small area at a time when R is small and more MBSPs are needed to complete the mission. With the increase of R, the number of MBSPs

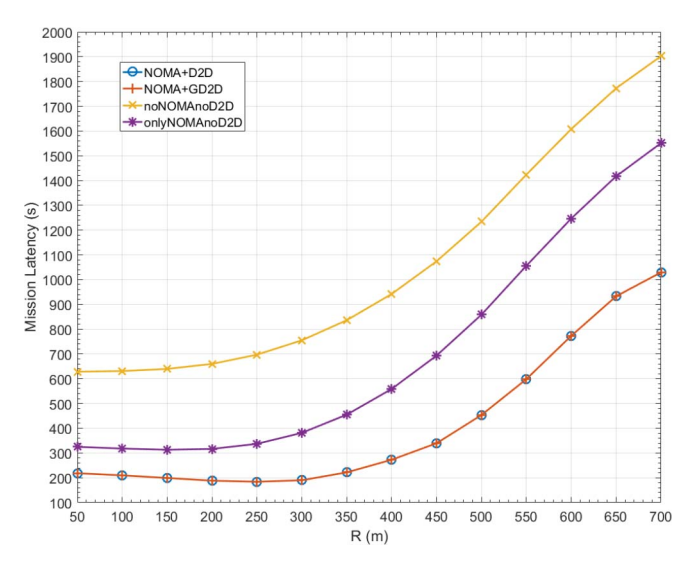


Fig. 12. Mission latency comparison with different schemes when the UAV dispatches FBs during its flying.

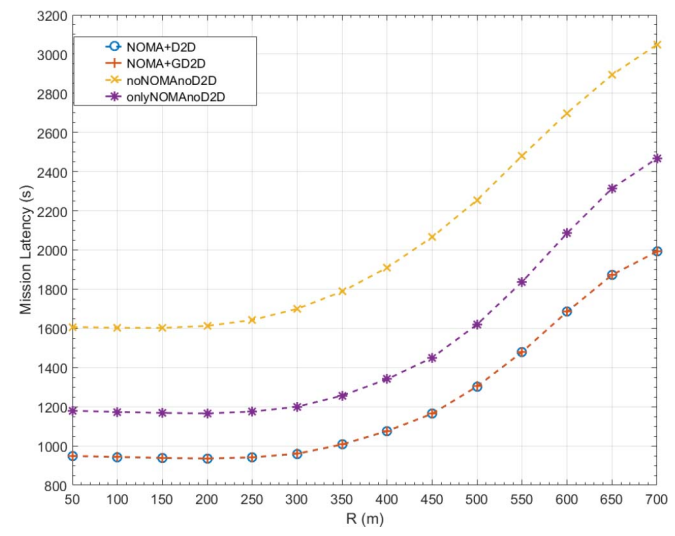


Fig. 13. Mission latency comparison with different schemes when the UAV flies to the location of each MBSP and hovers for file dispatching.

can be reduced. Hence, the UAV's flying path is shortened and more GUEs can be covered at the same time, resulting in a smaller  $T_{\text{total}}$ . However, although the number of MBSPs decreases with the further increasing of R, the GUEs that are far away from the UAV are also included in the coverage. Thus, the transmission rate becomes lower, and the UAV has to fly at a lower speed to ensure the correct file dispatching, resulting in an increased  $T_{\text{total}}$ . At the same time, it can be seen that the mission latency of the noNOMAnoD2D scheme almost keeps increasing with the increase of R. This is because the noNOMAnoD2D scheme does not have any assistance, and thus, the UAV has to wait for the finish of file transmission, no matter how far away the GUE is from the UAV and how bad the channel state is, resulting in big time consuming. While the efficiency of the onlyNOMAnoD2D scheme is between that of the other two schemes because of the use of NOMA.

Fig. 13 shows the case that the UAV flies to the location of each MBSP and hovers for file dispatching. The curves in

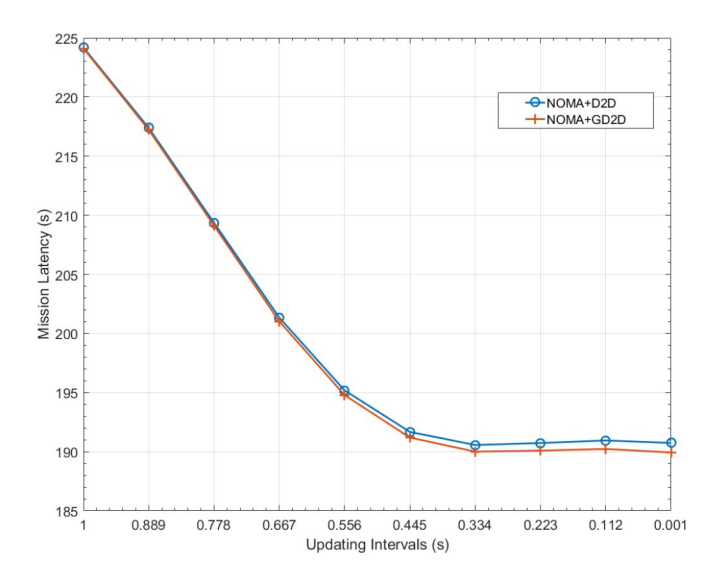


Fig. 14. Mission latency comparison with different schemes when the UAV dispatches FBs during its flying.

Fig. 13 show the same trend as that of Fig. 12. But in Fig. 13, the total mission latency increases sharply with the increase of R, due to the waste of flying time.

In addition, we also simulate the performance under different updating intervals, which is shown in Fig. 14. As we can see that the mission latency decreases with the decrease of updating interval because a shorter updating interval makes the current resource allocation more suitable for the real channel conditions. When the updating interval further decreases, the mission latency will no longer decrease because the updating interval is small enough for the variation of channel state. Therefore, the updating interval should be set based on the actual situation. It will not bring expected improvement of the performance but increase the system processing load in vain if the updating interval is set too small.

Fig. 15 shows the influence of the GUEs' movement. We assume that each GUE moves in a random direction along the axis and has fixed speed  $v_g$ . As we can see in Fig. 15, with the growing of  $v_g$ , the mission latency becomes larger. When the GUEs cannot move quickly, the system performance has not been greatly affected, because most of the GUEs are still in their original circles and no additional time-wasting operation is needed. When the GUEs have higher speed, it takes more time to complete the mission because some of the GUEs are out of their own circles. This makes the GUEs that are not in any circle receive their file data through D2D only, which seriously affects the efficiency of the system but reduces the load of NOMA links, and less GUEs can participate in the NOMA transmission, which makes the UAV can fly at a higher speed, thus the increased mission latency can be offset to some extent.

Through all these simulation results, it is verified that the performance of our proposed GFD protocol is in line with the expectation. Next, we discuss the possibility of applying the proposed GFD protocol to the real environment. First, the investigated UAV communication scenario has a lot of practical applications as described in Sections I and III. Second, our proposed GFD protocol is designed completely based on

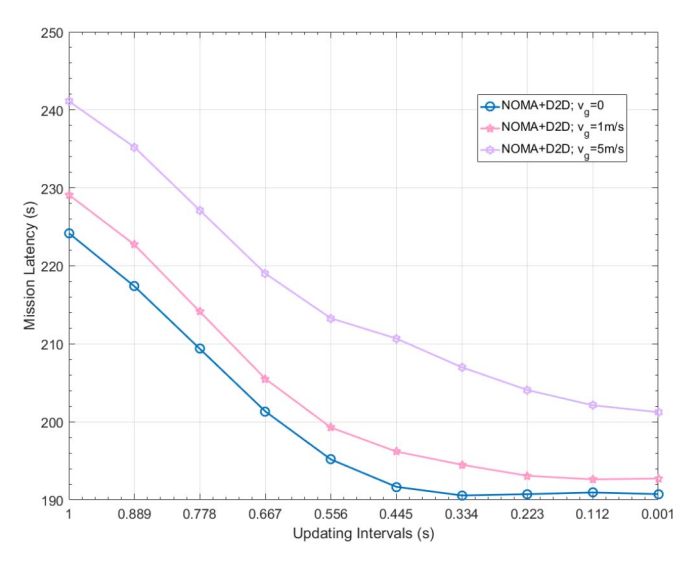


Fig. 15. Mission latency comparison with different velocities of GUEs.

strict derivation, following the basic physical concepts and mathematical logic as described in Section IV. Finally, in the simulations, all the parameters are set based on practical scenarios. Therefore, our proposed GFD protocol designed through such a reliable procedure can be feasible in practical applications as well.

#### VI. CONCLUSION

In this article, we investigated the mission latency minimization problem in the UAV-NOMA networks, where NOMA, D2D, and resource sharing based on spatial reuse were employed to improve the network performance. In order to solve the optimization problem efficiently, we divided the problem into three subproblems and further proposed the GFD protocol. In the proposed GFD protocol, the UAV dispatched files during its flying using NOMA. The GUEs were allowed to share FBs using D2D via the same RB used by NOMA links under interference management. Graph-based algorithms were utilized in the processes of NOMA user grouping and interference management. The simulation results verified the efficiency of the proposed GFD protocol.

#### REFERENCES

- S. Zhang, Y. Zeng, and R. Zhang, "Cellular-enabled UAV communication: A connectivity-constrained trajectory optimization perspective," IEEE Trans. Commun., vol. 67, no. 3, pp. 2580–2604, Mar. 2019.
- [2] H. Wang, J. Wang, J. Chen, Y. Gong, and G. Ding, "Network-connected UAV communications: Potentials and challenges," *China Commun.*, vol. 15, no. 12, pp. 111–121, Dec. 2018.
- [3] X. Yuan et al., "Capacity analysis of UAV communications: Cases of random trajectories," *IEEE Trans. Veh. Technol.*, vol. 67, no. 8, pp. 7564–7576, Aug. 2018.
- [4] A. Guidotti et al., "Architectures and key technical Challenges for 5G systems incorporating satellites," *IEEE Trans. Veh. Technol.*, vol. 68, no. 3, pp. 2624–2639, Mar. 2019.
- [5] C. Cicek, H. Gultekin, B. Tavli, and H. Yanikomeroglu, "UAV base station location optimization for next generation wireless networks: Overview and future research directions," in *Proc. 1st Int. Conf. UVS*, Muscat, Oman, Feb. 2019, pp. 1–16.
- [6] "Enhanced LTE support for aerial vehicles," 3GPP, Sophia Antipolis, France, Rep. TR 36.777, 2017. [Online]. Available: http://www.3gpp.org/ftp//Specs/archive/36\_series /36.777/

- [7] "Study on new radio (NR) to support non-terrestrial networks," 3GPP, Sophia Antipolis, France, Rep. TR 38.811, 2019. [Online]. Available: http://www.3gpp.org/ftp// Specs/archive/38\_series/38.811/
- [8] M. Mozaffari, W. Saad, M. Bennis, and M. Debbah, "Mobile Internet of Things: Can UAVs provide an energy-efficient mobile architecture?" in *Proc. IEEE Global Commun. Conf. (GLOBECOM)*, Washington, DC, USA, Dec. 2016, pp. 1–6.
- [9] Y. Li, B. Yang, Z. Chen, C. Chen, and X. Guan, "A contract-Stackelberg offloading incentive mechanism for vehicular parked-edge computing networks," in *Proc. IEEE Veh. Technol. Conf.*, Kuala Lumpur, Malaysia, Apr. 2019, pp. 1–5.
- [10] Z. Huang, X. Zhang, and X. Cheng, "A new non-geometrical stochastic model for non-stationary wideband vehicular communication channels," *IET Commun.*, vol. 14, no. 1, pp. 54–62, Jan. 2020.
- [11] X. Cheng, R. Zhang, and L. Yang, "Wireless towards the era of intelligent vehicles," *IEEE Internet Things J.*, vol. 6, no. 1, pp. 188–202, Feb. 2019.
- [12] X. Cheng, Y. Li, and L. Bai, "UAV communication channel measurement, modeling, and application," *J. Commun. Inf. Netw.*, vol. 4, no. 4, pp. 32–43, Dec. 2019.
- [13] X. Cheng and Y. Li, "A 3-D geometry-based stochastic model for UAV-MIMO wideband nonstationary channels," *IEEE Internet Things* J., vol. 6, no. 2, pp. 1654–1662, Apr. 2019.
- [14] Z. Ding, X. Lei, G. K. Karagiannidis, R. Schober, J. Yuan, and V. K. Bhargava, "A survey on non-orthogonal multiple access for 5G networks: Research challenges and future trends," *IEEE J. Sel. Areas Commun.*, vol. 35, no. 10, pp. 2181–2195, Oct. 2017.
- [15] L. Dai, B. Wang, Y. Yuan, S. Han, C.-L. I, and Z. Wang, "Non-orthogonal multiple access for 5G: Solutions, challenges, opportunities, and future research trends," *IEEE Commun. Mag.*, vol. 53, no. 9, pp. 74–81, Sep. 2015.
- [16] Z. Ding, Z. Yang, P. Fan, and H. V. Poor, "On the performance of non-orthogonal multiple access in 5G systems with randomly deployed users," *IEEE Signal Process. Lett.*, vol. 21, no. 12, pp. 1501–1505, Dec. 2014.
- [17] Z. Wu, K. Lu, C. Jiang, and X. Shao, "Comprehensive study and comparison on 5G NOMA schemes," *IEEE Access*, vol. 6, pp. 18511–18519, 2018.
- [18] C. Chen, B. Wang, and R. Zhang, "Interference hypergraph-based resource allocation (IHG-RA) for NOMA-integrated V2X networks," *IEEE Internet Things J.*, vol. 6, no. 1, pp. 161–170, Feb. 2019.
- [19] B. Wang, R. Zhang, C. Cheng, X. Cheng, and L. Yang, "Interference hypergraph-based resource allocation (IHG-RA) for NOMA-integrated V2X networks," in *Proc. IEEE Global Commun. Conf. (GLOBECOM)*, Abu Dhabi, UAE, Dec. 2018, pp. 1–6.
- [20] K. Doppler, M. Rinne, C. Wijting, C. Ribeiro, and K. Hugl, "Device-to-device communication as an underlay to LTE-Advanced networks," *IEEE Commun. Mag.*, vol. 47, no. 12, pp. 42–49, Dec. 2009.
- [21] R. Zhang, X. Cheng, L. Yang, and B. Jiao, "Interference graph-based resource allocation (InGRA) for D2D communications underlaying cellular networks," *IEEE Trans. Veh. Technol.*, vol. 64, no. 8, pp. 3844–3850, Aug. 2015.
- [22] H. Tang and Z. Ding, "Mixed mode transmission and resource allocation for D2D communication," *IEEE Trans. Wireless Commun.*, vol. 15, no. 1, pp. 162–175, Jan. 2016.
- [23] X. Cheng, L. Yang, and X. Shen, "D2D for intelligent transportation systems: A feasibility study," *IEEE Trans. Intell. Trans. Syst.*, vol. 16, no. 4, pp. 1784–1793, Jan. 2015.
- [24] M. Alzenad, A. El-Keyi, and H. Yanikomeroglu, "3-D placement of an unmanned aerial vehicle base station for maximum coverage of users with different QoS requirements," *IEEE Wireless Commun. Lett.*, vol. 7, no. 1, pp. 38–41, Feb. 2018.
- [25] M. Mozaffari, W. Saad, M. Bennis, and M. Debbah, "Unmanned aerial vehicle with underlaid device-to-device communications: Performance and tradeoffs," *IEEE Trans. Wireless Commun.*, vol. 15, no. 6, pp. 3949–3963, Jun. 2016.
- [26] Z. Wang, L. Duan, and R. Zhang, "Adaptive deployment for UAV-aided communication networks," *IEEE Trans. Wireless Commun.*, vol. 18, no. 9, pp. 4531–4543, Sep. 2019.
- [27] Y. Zeng, X. Xu, and R. Zhang, "Trajectory design for completion time minimization in UAV-enabled multicasting," *IEEE Trans. Wireless Commun.*, vol. 17, no. 4, pp. 2233–2246, Apr. 2018.
- [28] Y. Zeng and R. Zhang, "Energy-efficient UAV communication with trajectory optimization," *IEEE Trans. Wireless Commun.*, vol. 16, no. 6, pp. 3747–3760, Jun. 2017.

- [29] D. Yang, Q. Wu, Y. Zeng, and R. Zhang, "Energy tradeoff in ground-to-UAV communication via trajectory design," *IEEE Trans. Veh. Technol.*, vol. 67, no. 7, pp. 6721–6726, Jul. 2018.
- [30] G. Zhang, H. Yan, Y. Zeng, M. Cui, and Y. Liu, "Trajectory optimization and power allocation for multi-hop UAV relaying communications," *IEEE Access*, vol. 6, pp. 48566–48576, 2018.
- [31] N. Zhao et al., "Joint trajectory and precoding optimization for UAV-assisted NOMA networks," *IEEE Trans. Commun.*, vol. 67, no. 5, pp. 3723–3735, May 2019.
- [32] Y. Liu, Z. Qin, Y. Cai, Y. Gao, G. Y. Li, and A. Nallanathan, "UAV communications based on non-orthogonal multiple access," *IEEE Wireless Commun.*, vol. 26, no. 1, pp. 52–57, Feb. 2019.
- [33] M. Sohail, C. Leow, and S. Won, "Non-orthogonal multiple access for unmanned aerial vehicle assisted communication," *IEEE Access*, vol. 6, pp. 22716–22727, 2018.
- [34] H. He, S. Zhang, Y. Zeng, and R. Zhang, "Joint altitude and beamwidth optimization for UAV-enabled multiuser communications," *IEEE Commun. Lett.*, vol. 22, no. 2, pp. 344–347, Feb. 2018.
- [35] L. Yuan, J. Pan, N. Yang, Z. Ding, and J. Yuan, "Successive interference cancellation for LDPC coded nonorthogonal multiple access systems," *IEEE Trans. Veh. Technol.*, vol. 67, no. 6, pp. 5460–5464, Jun. 2018.
- [36] B. Ling, C. Dong, J. Dai, and J. Lin, "Multiple decision aided successive interference cancellation receiver for NOMA systems," *IEEE Wireless Commun. Lett.*, vol. 6, no. 4, pp. 498–501, Aug. 2017.
- [37] D. W. Matolak and R. Sun, "Unmanned aircraft systems: Air-ground channel characterization for future applications," *IEEE Veh. Technol. Mag.*, vol. 10, no. 2, pp. 79–85, Jun. 2015.
- [38] D. Tse and P. Viswanath, Fundamentals of Wireless Communication. Cambridge, U.K.: Cambridge Univ. Press, 2005.
- [39] A. Srinivas, G. Zussman, and E. Modiano, "Construction and maintenance of wireless mobile backbone networks," *IEEE/ACM Trans. Netw.*, vol. 17, no. 1, pp. 239–252, Feb. 2009.
- [40] J. Lyu, Y. Zeng, R. Zhang, and T. J. Lim, "Placement optimization of UAV-mounted mobile base stations," *IEEE Commun. Lett.*, vol. 21, no. 3, pp. 604–607, Mar. 2017.
- [41] Traveling Salesman Problem: Solver-Based. Accessed: Jul. 22, 2017. [Online]. Available: https://www.mathworks.com/help/optim/ug/ travelling-salesman-problem.html
- [42] G. Laporte, "The traveling salesman problem: An overview of exact and approximate algorithms," EUR. J. Oper. Res., vol. 59, no. 2, pp. 231–247, Jun. 1992.
- [43] A. H. Alaidi and A. Mahmood, "Distributed hybrid method to solve multiple traveling salesman problems," in *Proc. ICASEA*, Wasit, Iraq, Mar. 2018, pp. 74–78.
- [44] M. S. Ali, H. Tabassum, and E. Hossain, "Dynamic user clustering and power allocation for uplink and downlink non-orthogonal multiple access (NOMA) systems," *IEEE Access*, vol. 4, pp. 6325–6343, 2016.
- [45] L. Chen, L. Ma, and Y. Xu, "Proportional fairness-based user pairing and power allocation algorithm for non-orthogonal multiple access system," *IEEE Access*, vol. 7, pp. 19602–19615, 2019.
- [46] Z. Ding, M. Peng, and H. V. Poor, "Cooperative non-orthogonal multiple access in 5G systems," *IEEE Commun. Lett.*, vol. 19, no. 8, pp. 1462–1465, Jun. 2015.
- [47] S. Sarkar and K. N. Sivarajan, "Hypergraph models for cellular mobile communication systems," *IEEE Trans. Veh. Technol.*, vol. 47, no. 2, pp. 460–471, May 1998.
- [48] R. Zhang, X. Cheng, Q. Yao, C.-X. Wang, Y. Yang, and B. Jiao, "Interference graph-based resource-sharing schemes for vehicular networks," *IEEE Trans. Veh. Technol.*, vol. 62, no. 8, pp. 4028–4039, Oct. 2013.
- [49] L. Liang, S. Xie, G. Y. Li, Z. Ding, and X. Yu, "Graph-based resource sharing in vehicular communication," *IEEE Trans. Wireless Commun.*, vol. 17, no. 7, pp. 4579–4592, Jul. 2018.
- [50] Q. Wang, Z. Chen, J. Cai, and Z. Tian, "Establishing UAV-aided VBSs for secure multicasting," *IEEE Wireless Commun. Lett.*, early access, Mar. 3, 2020, doi: 10.1109/LWC.2020.2978076.
- [51] J. Li et al., "Joint optimization on trajectory, altitude, velocity, and link scheduling for minimum mission time in UAV-aided data collection," *IEEE Internet Things J.*, vol. 7, no. 2, pp. 1464–1475, Feb. 2020.



**Baoji Wang** received the B.S. degree from Nankai University, Tianjin, China, in 2015. He is currently pursuing the Ph.D. degree with the State Key Laboratory of Advanced Optical Communication Systems and Networks, School of EECS, Peking University, Beijing, China.

His research interests include communication signal processing, vehicular communications and networking, and UAV communications.

Dr. Wang has received the Best Paper Awards at GLOBECOM'18.



**Rongqing Zhang** (Member, IEEE) received the B.S. and Ph.D. degrees (Hons.) from Peking University, Beijing, China, in 2009 and 2014, respectively.

From 2014 to 2018, he worked as a Postdoctoral Research Fellow with Colorado State University, Fort Collins, CO, USA. Since 2019, he has been an Associate Professor with Tongji University, Shanghai, China. He has authored and coauthored two books, two book chapters, and over 100 papers in refereed journals and conference proceedings. His current research interests include physical layer

security, vehicular communications and networking, UAV communications, and autonomous driving.

Dr. Zhang was a recipient of the Academic Award for Excellent Doctoral Students, Ministry of Education of China, the co-recipient of the First-Class Natural Science Award, Ministry of Education of China, and received the Best Paper Awards at IEEE ITST'12, ICC'16, GLOBECOM'18, and ICC'19. He was also awarded as an International Presidential Fellow of Colorado State University in 2017. He is currently serving as an Associate Editor for *IET Communications* and *Complexity* (Hindawi).



**Chen Chen** (Senior Member, IEEE) received the Ph.D. degree from Peking University, Beijing, China, in 2009.

He is currently an Associate Professor with Peking University. Since 2010, he has been the Principal Investigator of over 20 funded research projects. He has authored or coauthored over 100 journal and conference papers and four books. His current research interests include signal processing, and wireless communications and networking.

Dr. Chen was a recipient of two Outstanding

Paper Awards from the Chinese Government of Beijing in 2013 and 2018, respectively, and the Best Paper Awards at IEEE ICNC'17, ICCS'18, and Globecom'18. He is currently an Associate Editor of *IET Communications*. He has served as the symposium co-chair, the session chair, and a member of the Technical Program Committee for several international conferences.



Xiang Cheng (Senior Member, IEEE) received the Ph.D. degree from Heriot-Watt University, Edinburgh, U.K., and the University of Edinburgh, Edinburgh, in 2009.

He is currently a Professor with Peking University, Beijing, China, subject on which he has published more than 200 journal and conference papers, six books, and holds ten patents. His general research interests are in the areas of channel modeling, wireless communications, and data analytics.

Prof. Cheng was a recipient of the IEEE Asia–Pacific Outstanding Young Researcher Award in 2015 and the co-recipient of the 2016 IEEE JSAC Best Paper Award: Leonard G. Abraham Prize, the NSFC Outstanding Young Investigator Award, and the First-Rank and Second-Rank Award in Natural Science, Ministry of Education, in China. He has also received the Best Paper Awards at IEEE ITST'12, ICCC'13, ITSC'14, ICC'16, ICNC'17, GLOBECOM'18, ICCS'18, and ICC'19. He has served as the symposium leading chair, the co-chair, and a member of the Technical Program Committee for several international conferences. He is currently an Associate Editor of the IEEE TRANSACTIONS ON WIRELESS COMMUNICATIONS, the IEEE TRANSACTIONS ON INTELLIGENT TRANSPORTATION SYSTEMS, IEEE WIRELESS COMMUNICATIONS LETTERS, and the *Journal of Communications and Information Networks*, and is an IEEE Distinguished



**Liuqing Yang** (Fellow, IEEE) received the Ph.D. degree in electrical and computer engineering from the University of Minnesota, Minneapolis, MN, USA, in 2004.

She is currently a Professor with Colorado State University, Fort Collins, CO, USA. Her general interests are in communications and networking—subjects on which she has published more than 330 journal and conference papers, four book chapters, and five books.

Prof. Yang was a recipient of the ONR Young Investigator Program Award in 2007, and the NSF Faculty Early Career Development Award in 2009, and the Best Paper Award at IEEE ICUWB'06, ICCC'13, ITSC'14, GLOBECOM'14, ICC'16, WCSP'16, GLOBECOM'18, ICCS'18, and ICC'19. She is the Editor-in-Chief of *IET Communications*, an Executive Editorial Committee Member for the IEEE TRANSACTIONS ON COMMUNICATIONS, and a Senior Editor for the IEEE TRANSACTIONS ON SIGNAL PROCESSING. She has also served as an Editor for the IEEE TRANSACTIONS ON WIRELESS COMMUNICATIONS, the IEEE TRANSACTIONS ON INTELLIGENT TRANSPORTATION SYSTEMS, IEEE INTELLIGENT SYSTEMS, and *PHYCOM: Physical Communication*, and as the program chair, the track/symposium chair, or the TPC chair for many conferences.



**Hang Li** received the B.E. and M.S. degrees from Beihang University, Beijing, China, in 2008 and 2011, respectively, and the Ph.D. degree from Texas A&M University, College Station, TX, USA, in 2016.

He was a Postdoctoral Research Associate with Texas A&M University from September 2016 to August 2017 and the University of California at Davis, Davis, CA, USA, from September 2017 to March 2018. He was a Visiting Research Scholar with the Shenzhen Research Institute of Big Data,

Shenzhen, China, from April 2018 to June 2019, where he has been a Research Scientist since June 2019. His current research interests include wireless networks, Internet of Things, stochastic optimization, and applications of machine learning.



**Ye Jin** received the B.E. and M.S. degrees from Peking University, Beijing, China, in 1986 and 1989, respectively.

He is currently a Professor with the Institute of Modern Communications, Peking University. He has been the Principal Investigator of over 30 funded research projects. His general research interests are in the areas of satellite and wireless communications and networking.

Prof. Jin was a recipient of the First Prize of the National Science and Technology Progress Awards of China.